



## Speleothem record of the last 180 ka in Villars cave (SW France): Investigation of a large $\delta^{18}\text{O}$ shift between MIS6 and MIS5

K. Wainer<sup>a,b,\*</sup>, D. Genty<sup>a</sup>, D. Blamart<sup>c</sup>, M. Daëron<sup>c</sup>, M. Bar-Matthews<sup>d</sup>, H. Vonhof<sup>e</sup>, Y. Dublyansky<sup>f</sup>, E. Pons-Branchu<sup>a</sup>, L. Thomas<sup>g</sup>, P. van Calsteren<sup>g</sup>, Yves Quinif<sup>h</sup>, N. Caillon<sup>c</sup>

<sup>a</sup>Laboratoire des Sciences du Climat et de l'Environnement, UMR CEA/CNRS/UVSQ1572 Bat 701, L'Orme des Merisiers CEA Saclay, 91 191 Gif sur Yvette cedex, France

<sup>b</sup>Geoazur, Université de Nice-Sophia-Antipolis, UMR6526, La Darse, B.P. 48, 06235 Villefranche/Mer, France

<sup>c</sup>Laboratoire des Sciences du Climat et de l'Environnement, UMR CEA/CNRS/UVSQ1572 Bat 12, avenue de la Terrasse, 91 198 Gif sur Yvette cedex, France

<sup>d</sup>Geological Survey of Israël, 30 Malchei Israel St, Jerusalem 95501, Israël

<sup>e</sup>Departement of Sedimentology and Marine Geology Faculty of Earth and life sciences, Vrije Universiteit Amsterdam, De Boelelaan 1085, 1081HV Amsterdam, The Netherlands

<sup>f</sup>Institut für Geologie und Paläontologie, Leopold-Franzens-Universität Innsbruck, Innrain 52, 6020 Innsbruck, Austria

<sup>g</sup>Department of Earth and Environmental Sciences, The Open University, Milton Keynes MK7 6AA, UK

<sup>h</sup>Institut Jules Cornet (Géologie), Faculté Polytechnique de Mons, Rue de Houdain, 9, 7000 Mons, Belgium

### ARTICLE INFO

#### Article history:

Received 8 January 2010

Received in revised form

30 June 2010

Accepted 1 July 2010

### ABSTRACT

The Vil-car-1 flowstone core from Villars cave (SW France) provides one of the first European speleothem records extending back to 180 ka, based on U–Th TIMS and MC-ICP-MS measurements. The core offers a continuous record of Termination II and the Last Interglacial. The penultimate deglaciation is characterized by a prominent 5‰ depletion in calcite  $\delta^{18}\text{O}$ . Determining which specific environmental factors controlled such a large oxygen isotopic shift offers the opportunity to assess the impact of various factors influencing  $\delta^{18}\text{O}$  variations in speleothem calcite.

Oxygen isotope analyses of fluid inclusions indicate that drip water  $\delta^{18}\text{O}$  remained within a very narrow range of  $\pm 1\%$  from Late MIS6 to the MIS5  $\delta^{18}\text{O}$  optimum. The possibility of such a stable behaviour is supported by simple calculations of various effects influencing seepage water  $\delta^{18}\text{O}$ .

Although this could suggest that the isotopic shift in calcite is mainly driven by temperature increase, attempts to quantify the temperature shift from Late MIS6 to the MIS5  $\delta^{18}\text{O}$  optimum by assuming an equilibrium relationship between calcite and fluid inclusion  $\delta^{18}\text{O}$  yield unreasonably high estimates of  $\sim 20^\circ\text{C}$  warming and Late MIS6 cave temperatures below  $0^\circ\text{C}$ ; this suggests that the flowstone calcite precipitated out of thermodynamic equilibrium at this site.

Using a method proposed by Guo et al. (submitted for publication) combining clumped isotope measurements, fluid inclusion and modern calcite  $\delta^{18}\text{O}$  analyses, it is possible to quantitatively correct for isotopic disequilibrium and estimate absolute paleotemperatures. Although the precision of these absolute temperature reconstructions is limited by analytical uncertainties, the temperature rise between Late MIS6 and the MIS5 optimum can be robustly constrained between  $13.2 \pm 2.6$  and  $14.6 \pm 2.6^\circ\text{C}$  ( $1\sigma$ ), consistent with existing estimates from Western Europe pollen and sea-surface temperature records.

© 2010 Elsevier Ltd. All rights reserved.

\* Corresponding author at: Laboratoire des Sciences du Climat et de l'Environnement, UMR CEA/CNRS/UVSQ1572 Bat 701, L'Orme des Merisiers CEA Saclay, 91 191 Gif sur Yvette cedex, France. Tel.: +33 1 69082866; fax: +33 1 69087716.

E-mail addresses: [karinewainer@gmail.com](mailto:karinewainer@gmail.com) (K. Wainer), [Dominique.genty@lsce.ipsl.fr](mailto:Dominique.genty@lsce.ipsl.fr) (D. Genty), [dominique.blamart@lsce.ipsl.fr](mailto:dominique.blamart@lsce.ipsl.fr) (D. Blamart), [mathieu@daeron.fr](mailto:mathieu@daeron.fr) (M. Daëron), [matthews@gsi.gov.il](mailto:matthews@gsi.gov.il) (M. Bar-Matthews), [vonh@falw.vu.nl](mailto:vonh@falw.vu.nl) (H. Vonhof), [juri.dublyanski@uibk.ac.at](mailto:juri.dublyanski@uibk.ac.at) (Y. Dublyansky), [Edwige.pons-branchu@lsce.ipsl.fr](mailto:Edwige.pons-branchu@lsce.ipsl.fr) (E. Pons-Branchu), [l.e.thomas@open.ac.uk](mailto:l.e.thomas@open.ac.uk) (L. Thomas), [P.V.calsteren@open.ac.uk](mailto:P.V.calsteren@open.ac.uk) (P. van Calsteren), [Yves.Quinif@fpms.ac.be](mailto:Yves.Quinif@fpms.ac.be) (Y. Quinif), [nicolas.caillon@lsce.ipsl.fr](mailto:nicolas.caillon@lsce.ipsl.fr) (N. Caillon).

### 1. Introduction

Climate variations are driven by a complex combination of factors such as orbital parameters, interactions between atmospheric and ocean circulation, greenhouse gas effects, and system feedbacks. Physically deciphering these various influences is one of the main goals for climatologists.

The penultimate deglaciation (Termination II, or TII; a period between 135 and 125 ka before present) one of the closest termination to the present day interglacial, occurred under orbital parameters different from the more recent Termination I (TI). Thus,

characterizing this deglaciation is of first importance in order to better constrain the influence of orbital parameters on major climatic variations. Several studies based on different archives cover the TII period but few provide quantitative climatic data. Antarctic records such as the Vostok ice core cover several climatic cycles but their temporal resolution is low and the associated age models suffer from significant uncertainties. Nevertheless, deuterium excess records from such core can be used to quantify local temperature variations, including during Termination II (Vimeux et al., 2002). At lower latitudes, studies of Chinese speleothems provide a record of East-Asian monsoon strength with a well constrained chronology but these studies do not provide temperature estimates (e.g. Yuan et al., 2004; Cheng et al., 2006). In Western Europe, several sea-surface temperature (SST) records covering this key period were recovered from the Alboran sea and the Iberian Margin (mean annual SST derived from the  $U_{37}$  alkenone index: (Shackleton et al., 2002; Martrat et al., 2004, 2007)), the Bay of Biscay and offshore West Ireland (seasonal SST deduced from foraminifera assemblages (Kandiano et al., 2004; Sánchez Goñi et al., 2008)). Quantified paleo-climate reconstructions of continental settings for TII exist but they remain scarce and often entail large uncertainties. The longest high resolution and continuous continental record in the area of interest (Western Europe and Mediterranean basin) was obtained from speleothems in Soreq cave (Israel), and covers the last 177 ka. According to several studies involving fluid inclusion  $\delta D$ , clumped isotope analyses and nearby marine cores (SST estimates from  $\delta^{18}O_{G.ruber}$  and alkenones), carbonate  $\delta^{18}O$  variations through time in Soreq Cave reflect a combination of source isotopic composition, temperature and amount effect variations (Matthews et al., 2000; Bar-Matthews et al., 2003; McGarry et al., 2004; Affek et al., 2008; Almogi-Labin et al., 2009). Among other important results, these studies estimate the glacial/interglacial temperature rise in the region at  $\sim 7^\circ C$  (Affek et al., 2008). The Corchia cave in Italy provides speleothem records of the penultimate deglaciation with a well constrained U–Th chronology, allowing precise tuning with Iberian Margin marine records (Drysdale et al., 2005, 2009); these studies date the inception of TII at  $141.0 \pm 2.5$  ka and abrupt warming of the deglaciation at  $133 \pm 2.5$  ka (mid-point). Over continental Western Europe, only a few quantified climate reconstructions have been established for the last climate cycle. Among them, the Monticchio Maar multiproxy record from South Italy (Brauer et al., 2007; Allen and Huntley, 2009) has a well constrained chronology based on radiometric dating and varve counting, covering the last 132 ka. Alternatively, the Velay lake record from southern France provides quantified estimates of temperature and rainfall over the last four

glacial cycles, although its chronology is not as well constrained as that of the Monticchio record, and is the closest to our study site ( $\sim 300$  km east from Villars, (Beaulieu et al., 1991; Cheddadi et al., 2005)). Pollen assemblages recovered from marine cores around Western Europe also allow reconstructions of terrestrial climate (e.g. Combourieu-Nebout et al., 2002; Sánchez Goñi et al., 2005). In summary, there is currently very limited quantitative data covering the penultimate deglaciation in Western Europe.

We present here a speleothem stable isotope profile ( $\delta^{13}C_c$  and  $\delta^{18}O_c$ ) recovered from a flowstone drill core in Villars cave (SW France), which provides a discontinuous record of the last 180 ka. The oxygen profile exhibits a striking  $-5\text{‰}$  drop in calcite  $\delta^{18}O$  coeval with the penultimate deglaciation, similar to the Soreq cave record. The present study focuses on this major climatic transition, aiming to characterize it quantitatively through the use of various analytical techniques: measurements of calcite stable isotopic compositions (C–O), trace elements relative concentrations (e.g., Mg, Sr), stable isotopic compositions of fluid inclusions (H–O), and calcite clumped isotopes ( $\Delta_{47}$ ). Combination of these methods enables us to estimate the amplitude of the temperature rise between the end of the penultimate glacial and the last interglacial optimum and to understand the sharp drop of the calcite  $\delta^{18}O_c$  values during Termination II. The consequences in terms of paleo-dripwater oxygen isotopic composition ( $\delta^{18}O_w$ ) and the different controls on the oxygen isotopic composition of the calcite ( $\delta^{18}O_c$ ) in Villars Cave will be discussed.

## 2. Site and sample description

### 2.1. Villars cave site

Villars cave is located in south-west France, about 200 km inland from the Atlantic coast ( $45^\circ 30'N$ ,  $0^\circ 50'E$ , 175 masl; Fig. 1). The local climate is oceanic temperate with mild and humid winters. The surface atmospheric mean annual temperature is  $12.1 \pm 0.7^\circ C$  (Sept. 1984–Aug. 2007, data from Nontron meteorological station (Genty et al., 2006; Wainer et al., 2009)) with average temperatures of  $6.4 \pm 1.3^\circ C$  in the winter (January–March) and  $18.8 \pm 1.1^\circ C$  in the summer (July–September). Total annual rainfall ( $1020 \pm 206$  mm) varies from year to year but is distributed rather uniformly throughout each year. Because the soil cover is thin (0–20 cm) and the karstic network is densely fissured, stalactite drip rates slow down during the summer, but infiltration persists even when monthly theoretical evapotranspiration estimates exceed monthly amounts of rainfall (Genty et al., 2006; Genty, 2008). However, in spite of the seasonal variability of stalactite drip rates, the  $\delta^{18}O$  values of the drip water remain fairly stable and closely approximate the (amount-weighted) average  $\delta^{18}O$  composition of meteoric waters ( $-6.33 \pm 0.18\text{‰}$ ); (Genty et al., 2006; Genty, 2008). Local vegetation cover consists of a deciduous forest comprising juniper, oak and hornbeam trees (C3 type vegetation).

The Villars cave system lies within a Bathonian–Bajocian oolitic limestone, at depths of 10–40 m depth. The cave network is 10 km long and organized into two levels (upper and lower), consisting of small galleries with a few larger chambers. The mean temperature in the upper galleries is  $12.4 \pm 0.4^\circ C$ , oscillating seasonally with a time lag of a more than a month relative to the surface temperature. The lower galleries, by contrast, do not experience any significant seasonal variation in temperature, remaining at  $11.6 \pm 0.1^\circ C$  (Genty, 2008).

### 2.2. Flowstone core Vil-car-1

The flowstone core Vil-car-1 (7.5 cm diameter, 114.2 cm long) was drilled by Y. Quinif and D. Genty in 1998 in a decametric large

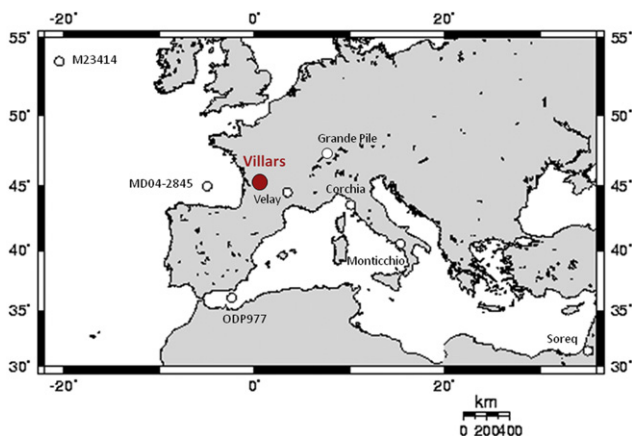


Fig. 1. Sites locations.

chamber (“chambre du Blacon”) about 150 m from the nearest entrance, at a depth of  $\sim 25$  m below ground. This chamber lies at the junction of the lower and upper galleries. Temperature measurements between July and October 2007 at the sampling site indicate a temperature of  $12.8 \pm 0.4$  °C ( $n = 3$ ). The ( $\sim 5$  m<sup>2</sup>) flowstone surrounds and gently slopes away from a large pillar. Local slope at the drill location is  $\sim 20^\circ$ . The flowstone surface was visibly wet at the time of sampling, which suggests that the speleothem was still active at that time.

Petrographic observations of the core material indicate that most of the calcite has a palisade columnar fabric. The petrography varies from dark compact to white porous laminated calcite including gours features at some places (Fig. 2). A particularly striking petrographic feature is the extremely dark translucent “grey” calcite visible between 63.5 and 50 cm from the top. Some detrital material (probably clay particles) can be observed between calcite layers at some places (Fig. 2). Until a few decades ago, an underground river was known to flow through the lower part of this chamber. It is thus likely that clay-rich intervals in the flowstone (25.4–42.4 cm/top and 99–108.8 cm/top) are the

consequence of flooding episodes. Detrital contamination makes these layers are difficult to date with U–Th methods.

### 3. Methods

#### 3.1. U–Th dating

In total, 42 samples were analyzed in different laboratories. In the early stages of this study, two assessment dates were measured at the LSCE (France) according to procedures described in (Plagnes et al., 2002). Eighteen samples were dated in the Geological Survey of Israel (GSI). Less than 2 g were ground to powder, dissolved in nitric acid and spiked with <sup>229</sup>Th–<sup>236</sup>U. The samples were then loaded into columns containing 2 ml Bio-Rad AG 1X8 200–400 mesh resin in order to separate U fraction and Th fraction. U–Th measurements were performed by multicollector inductively coupled plasma mass spectrometer (MC-ICP-MS) Nu instruments Ltd using an Aridus micro-concentric nebuliser. Analytical details are provided in (Vaks et al., 2006).

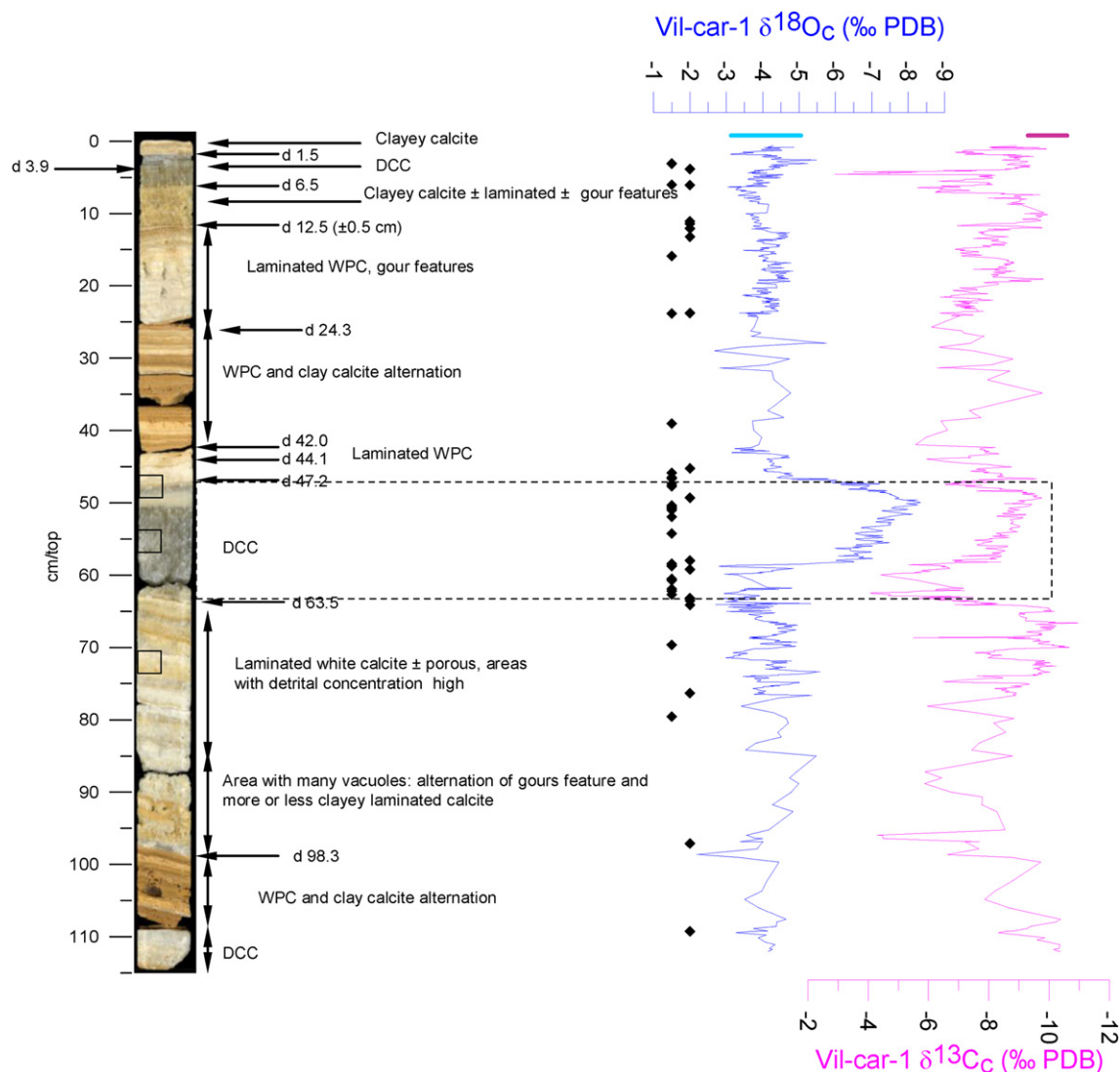


**Fig. 2.** Polished section of the core Vil-car-1 and description of the various deposits. DCC is for dark compact calcite and WPC for white porous calcite (Genty et al., 1997). Discontinuities are identified by the following code: d + depth in cm/top. On the right hand side, the  $\delta^{13}\text{C}$  (pink), the  $\delta^{18}\text{O}$  (blue) and the U–Th analysis location (black diamonds) are plotted versus the depth. Light blue and dark pink rectangles at the very top of the profiles indicate the modern day calcite composition in Villars Cave (Genty, 2008 and Unpublished). (For interpretation of the references to colour in this figure legend, the reader is referred to the web version of this article.)

Fourteen samples were dated at the GEOTOP-UQAM, Canada. Samples of 2–5 g of calcite were dissolved in nitric acid and spiked with  $^{229}\text{Th}$ – $^{236}\text{U}$ – $^{233}\text{U}$ . Uranium and thorium were separated in the anion exchange columns, as described in (Marshall et al., 2009). Both uranium and thorium fractions were loaded on pre-out-gassed single rhenium filaments with graphite coating. The measurements were made on a VG sector thermo-ionisation mass spectrometer fitted with an electrostatic filter and a Daly ion counter. U and Th isotopes were measured on the Daly detector.

Five samples were dated at the Open University (OU), UK. Fragments of 0.8–3 g were dissolved and spiked with  $^{229}\text{Th}$ – $^{236}\text{U}$  as described in (Edwards et al., 1987). Uranium was analyzed using single Re filament on thermo-ionization Finnigan MAT 262-RPQ-II mass spectrometer (McDermott et al., 1993; van Calsteren and Schwieters, 1995). Thorium was measured using bracketing technique on Nu plasma MC-ICP-MS (Turner et al., 2001).

### 3.2. Calcite stable isotopes measurements

Approximately 650 sub-samples were extracted along the growth direction of the flowstone using a 0.7 mm-diameter hand-held dental drill. In addition, samples were taken along 5 individual laminae at 11.55, 31.4, 47.45, 63.65, 97.45 cm/top to test for isotopic equilibrium, (“Hendy tests”; (Hendy, 1971; Schwarcz, 1986)). Resolution of sampling ranges from 0.5 to 5 mm. Most of the calcite isotope measurements  $\delta^{18}\text{O}_c$  and  $\delta^{13}\text{C}_c$  were made on a VG OPTIMA mass spectrometer at LSCE. Calcite was converted to  $\text{CO}_2$  through reaction with orthophosphoric acid at 90 °C. Fewer than 10% of measurements were made on a Finnigan  $\Delta+$  mass spectrometer (LSCE). Details of this technique are provided in (Govin et al., 2009).

Oxygen and carbon isotopic composition are normalized to VPDB standard. Analytical errors are 0.08‰ for  $\delta^{18}\text{O}_c$  and 0.05‰ for  $\delta^{13}\text{C}_c$  (2 $\sigma$ ).

### 3.3. Fluid inclusions stable isotope (H–O) analyses

The isotopic composition of percolating water from which the flowstone calcite precipitated can be determined by analyzing water released from fluid inclusions (FI) trapped within the carbonate matrix. Analyses were performed in two laboratories at Faculty of Earth and Life Sciences, Vrije Universiteit (VU) in Amsterdam and at the Institute for Geology and Palaeontology, Innsbruck University (IU). Both lines are based on the concept of Sharp et al. (2001) but employ slightly different techniques. Aliquots of calcite are crushed in a heated crusher (120–130 °C) under helium flow. Water released from inclusions and entrained by the helium flow is collected in a cryogenic trap. Upon completion of collection, water is released by flash-heating the trap and admitted into the high-temperature reactor of the standard thermal combustion/elemental analyzer (TC/EA) unit (Thermo Fisher Scientific). Molecular hydrogen and carbon monoxide evolved from water through reaction with glassy carbon at 1400 °C in the TC/EA reactor are separated in a chromatographic column and admitted, via a ConFlow II interface (Thermo Fisher Scientific), to an isotope-ratio mass spectrometer (Delta XP or Delta V Advantage; Thermo Fisher Scientific). Hydrogen is analyzed first, and, following a peak jump, the oxygen isotopic composition of carbon monoxide is determined subsequently in the same acquisition. Analytical uncertainties are  $\sim 1.5\%$  for  $\delta\text{D}$  and  $\sim 0.5\%$  for  $\delta^{18}\text{O}$  (1 $\sigma$ ). More detailed descriptions of both methods are given in (Vonhof et al., 2006, 2007) and (Dublyansky and Spötl, 2009).

Twelve samples were collected between 65 and 50 cm/top from twelve calcite layers. The masses of crushed sub-sample ranged

between 0.3 and 1.3 g; each layer was characterized by several replicate analyses. Analyses at VU were performed during three analytical periods (2006, 2007 and 2008), and measurements at IU were performed in one period (2009).

### 3.4. Trace element measurements

Between 72.20 and 43.20 cm/top from the top of the core, 103 analyses of trace elements were performed. Powder from samples drilled for stable isotope analyses was used for trace element studies. Some 30–60  $\mu\text{g}$  were dissolved in nitric acid ( $0.1 \text{ mol } \cdot \text{l}^{-1}$ ) at 20 or 40 ppm of calcium and measured on a Varian Vista Pro AX simultaneous inductively coupled plasma atomic emission spectrometer (ICP-AES) at the LSCE. Relative (normalized to Ca) concentrations of Mg, Sr, Ba, K, Na, Zn, Fe, Mn and Al were determined because they are most frequently found in the carbonates (e.g. Fairchild et al., 2000; Verheyden, 2001; Borsato et al., 2007) and have the potential to record paleo-hydrological conditions, speleothems growth rate, and processes such as prior calcite precipitation (Fairchild et al., 2006). For details of the method see (Cleroux et al., 2008; Greaves et al., 2008).

Concentrations of  $^{238}\text{U}$  and  $^{232}\text{Th}$  isotopes were measured in the course of the U–Th analyses. Because these isotopes are dominant in natural samples, their concentrations give a good approximation of the respective elemental contents.

## 4. Results

### 4.1. Stable isotopic composition of calcite

#### 4.1.1. Hendy test

The Hendy test is one of the most widely used tool to test whether calcite from a given stalagmite was deposited out of isotopic equilibrium (Hendy, 1971; Schwarcz, 1986). In this test both  $\delta^{18}\text{O}_c$  and  $\delta^{13}\text{C}_c$  are measured along an individual lamina, and usually plotted against the distance from the apex of the stalagmite.

Samples precipitated under thermodynamic equilibrium conditions are expected to display the following criteria: (a) no correlation between  $\delta^{18}\text{O}_c$  and  $\delta^{13}\text{C}_c$  along a single growth layer and (b)  $\delta^{18}\text{O}_c$  remains constant along a single growth layer while  $\delta^{13}\text{C}_c$  may vary irregularly.

The Hendy test is usually applied to stalagmites, eventually to stalactites (Vaks et al., 2006) but not on flowstone where the flowing path from a drop impact to the edge of the speleothem is difficult to define and, consequently, the possible isotopic enrichment difficult to constrain. However, we have applied it to five different flowstone laminae to check the isotopic composition behaviour laterally (Fig. 3a and b). The only lamina where we observed an arguably significant positive correlation between  $\delta^{18}\text{O}_c$  and  $\delta^{13}\text{C}_c$  (first Hendy criterion) is that located at 47.45 cm/top (Fig. 3a,  $R^2 = 0.8$ ). The  $\delta^{18}\text{O}_c$  and  $\delta^{13}\text{C}_c$  variations along laminae (second Hendy criterion) are shown in Fig. 3b: both  $\delta^{18}\text{O}_c$  and  $\delta^{13}\text{C}_c$  exhibit small variation along each lamina, varying within 0.7‰ (oxygen) and 0.6‰ (carbon).

#### 4.1.2. Oxygen isotope variations

Calcite oxygen isotopic composition fluctuates between  $-5.5$  and  $-2.2\%$  VPDB along the length of the core, except between 47 and 59 cm/top where  $\delta^{18}\text{O}_c$  values drop sharply by about  $-5\%$  between the extrema (Figs. 2 and 4). This large shift can be divided in two stages:

- (1) an abrupt depletion (from  $-2.9$  to  $-6.5\%$ ) with a short reversal ( $+2\%$  amplitude) centered on 59.1 cm/top (Figs. 2 and 4).

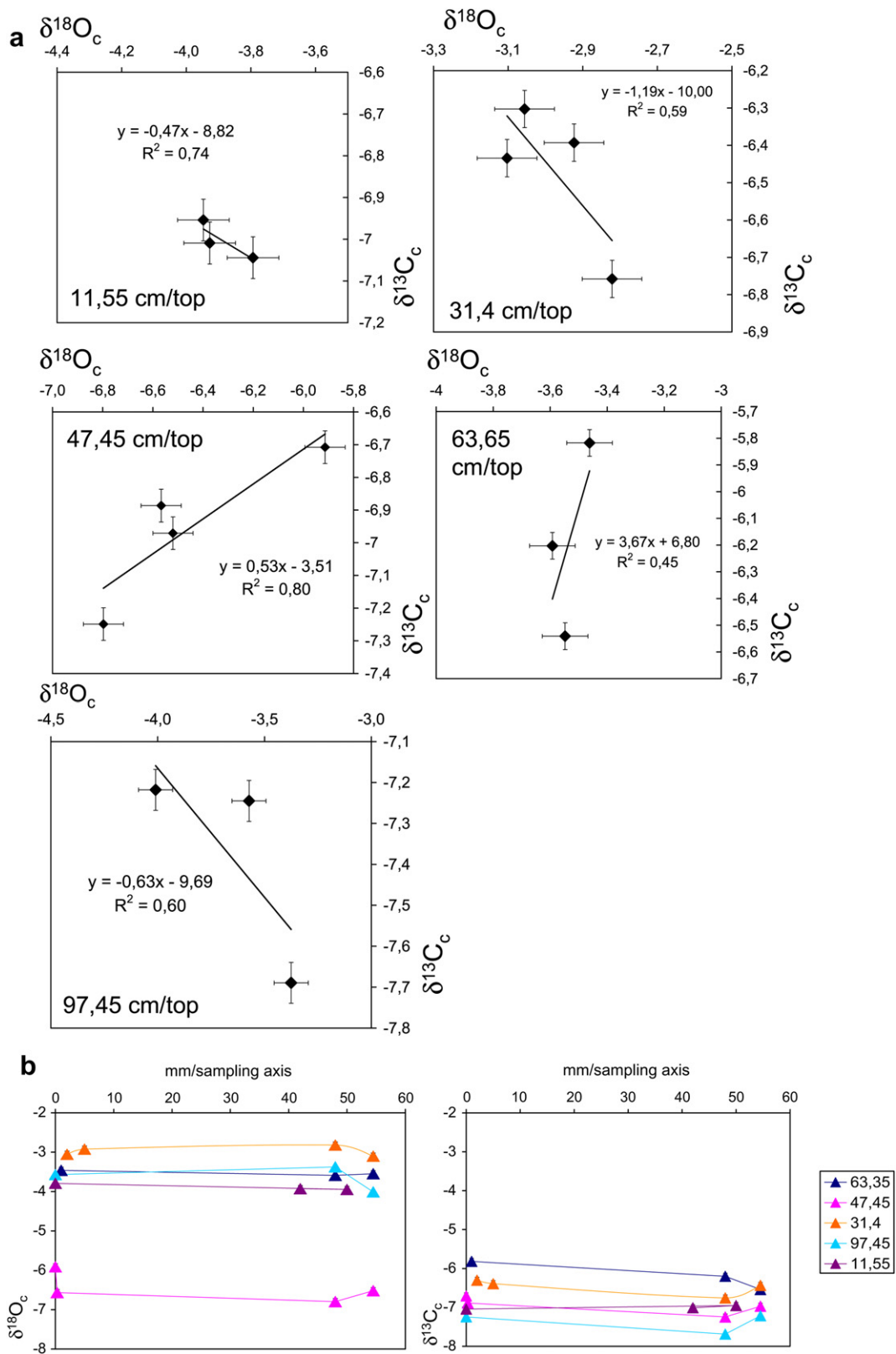
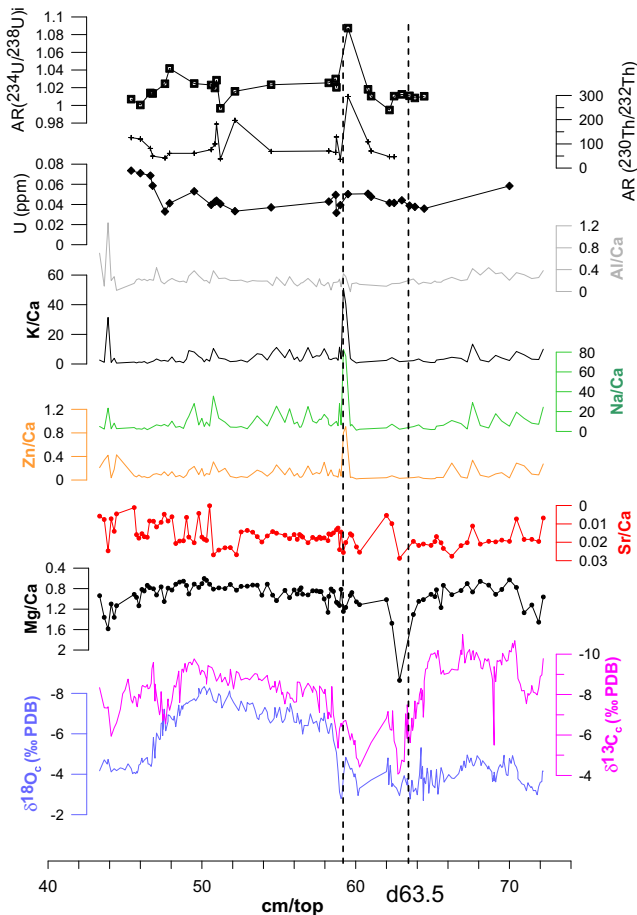


Fig. 3. Hendy test results a)  $\delta^{13}C_c$  vs  $\delta^{18}O_c$  for single laminae. b)  $\delta^{18}O_c$  and  $\delta^{13}C_c$  variability along single laminae versus distance from sampling axis.



**Fig. 4.** Comparison between Vil-car-1 carbon and oxygen isotopic composition with trace elements concentration (mmol/mol Ca), U concentration (ppm), ( $^{234}\text{U}/^{238}\text{U}$ ), and ( $^{230}\text{Th}/^{232}\text{Th}$ ) activity ratios between 75 and 40 cm/top. Dotted lines indicate d63.5 discontinuity located at 63.5 cm/top and the trace elements concentration peak.

(2) a more progressive depletion between 58.5 and 50.2 cm/top, culminating with the lightest overall  $\delta^{18}\text{O}_c$  value ( $-8.34\text{‰}$  at 50.15 cm/top). This progressive depletion is punctuated by second-order wiggles ( $\sim 0.8\text{‰}$  amplitude).

The subsequent enrichment is regular until  $-7.4\text{‰}$  at 48.8 cm/top and then both noisier and more abrupt to  $-4.4\text{‰}$  at 46.7 cm/top (Fig. 4).

#### 4.1.3. Carbon isotope variations

The overall  $\delta^{13}\text{C}_c$  record is much more variable along the core ranging between  $-11$  and  $-4\text{‰}$  (Figs. 2 and 4). In contrast to  $\delta^{18}\text{O}_c$ , the  $\delta^{13}\text{C}_c$  curve does not show a single peak but several ones. A negative peak between 59 and 47 cm/top corresponds to the main  $\delta^{18}\text{O}_c$  peak, but it does not stand out uniquely because other  $\delta^{13}\text{C}_c$  negative peaks exist, which do not correlate well with  $\delta^{18}\text{O}_c$  and display similar or even more depleted values (e.g. at  $\sim 70$  and 10 cm/top).

Calcite carbon isotopic variations appear positively correlated with  $\delta^{18}\text{O}_c$  variations during the oxygen excursion interval (59–47 cm/top): the abrupt depletion is between  $-4.4\text{‰}$  at 60.25 cm/top and  $-8.4\text{‰}$  at 58.45 cm/top for  $\delta^{13}\text{C}_c$  values and the progressive depletion leads to  $-9.76\text{‰}$  at 49.5 cm/top. This latter phase is also punctuated by second-order  $\delta^{13}\text{C}_c$  variations but these are less regular in frequency and amplitude (from 1.3 to  $0.3\text{‰}$ ) than the second-order oxygen oscillations in the same interval.

In summary, the Vil-car-1 isotopic record is characterized by a prominent and unique  $\delta^{18}\text{O}_c$  negative peak from 59 to 47 cm/top while the  $\delta^{13}\text{C}_c$  displays a more variable pattern.

#### 4.2. Trace elements

The aim of the trace element measurements is to help the understanding of local hydrology at the transition from MIS 6 to MIS 5 and to detect disturbances in the geochemical system that could be associated to age inversions (see below). We will focus on Mg, Sr, K, Na, Zn and Al concentrations because they give the most significant results.

The Ca-normalized K, Na, Zn and Al concentration vary slightly apart for shorts peaks (Fig. 4). The largest concentration peak centered at 59.35 cm/top, coincides with an isotopic event. Interestingly, concentrations in Sr, Mg and U, which are associated with the calcite lattice, do not display coeval major concentration changes, implying that aforementioned element concentration peak (K, Na, Al), which are not necessary directly associated to the calcite lattice is probably related to the presence of detrital matter brought via colloids and detrital particles (Borsato et al., 2007).

Strontium and magnesium concentrations show significant variability with relatively long term periods, the Mg concentration showing a close resemblance to the pattern of the  $\delta^{13}\text{C}_c$  variation.

Magnesium and strontium concentration are not correlated, attesting that no prior calcite precipitation has occurred (Fig. 4 (Fairchild et al., 2000)).

The Mg concentration peak centered at 62.85 cm/top is located just above a visual discontinuity, marked by a clay-rich layer and a petrographic change from white, porous to dark, dense calcite. This peak thus probably corresponds to a flushing episode occurring after a dry period (d63.5; Fig. 4).

#### 4.3. Dating results and age model

All U-series activity ratios presented in this paper are calculated using the decay constants published in (Cheng et al., 2000; Begemann et al., 2001) (Table 1). Uranium concentrations in studied sub-samples range from 18 to 74 ng/g. Twenty seven samples yield a relatively high detrital content ( $^{230}\text{Th}/^{232}\text{Th}$ )  $< 100$  (brackets denote activity ratio). Thus all ages were corrected for initial  $^{230}\text{Th}$  using a detrital activity ratio ( $^{230}\text{Th}/^{232}\text{Th}$ ) =  $0.9 \pm 0.45$  measured in “modern” Villars cave clay (Wainer et al., 2009). This correction results in ages younger by 0.3–15% (depending on the  $^{232}\text{Th}$  concentration) compared to their uncorrected values (Table 1).

The corrected ages are in stratigraphic order within uncertainty except during three intervals: (1) 6 to 5 cm/top; (2) 24 to 15 cm/top; and (3) 65 to 42 cm/top (Fig. 5 and Table 1). Samples from these intervals were analyzed independently in different laboratories using different techniques, which all yielded similar ages. We thus consider it unlikely that these apparent age reversals were caused by analytical artefacts (e.g. Th adsorption).

Our final age model was built upon the following assumptions:

- The detrital component has an activity ratio ( $^{230}\text{Th}/^{232}\text{Th}$ ) = 0.9, and remained constant through time (this correction being significant for 27 samples);
- The oldest ages for each depth are due to uranium leaching, in particular at the edge of discontinuities d63.5, d47.2, d42, d12.5 (Figs. 1 and 4), as proposed by (Lundberg and Ford, 1994).

The focus of the present study is on the interval between 65 and 42 cm/top. In some places within this interval, U concentration varies significantly within short intervals (for example, 32–50 ng/g

**Table 1**  
U–Th results. All quoted uncertainties are at 95% confidence level ( $2\sigma$ ).  $\delta^{234}\text{U} = ((^{234}\text{U}/^{238}\text{U})_{\text{activity ratio}} - 1) \times 1000$ . Decay constant used are  $9.1577 \times 10^{-6} \text{ yr}^{-1}$  for  $^{230}\text{Th}$ ,  $2.826 \times 10^{-6} \text{ yr}^{-1}$  for  $^{234}\text{U}$  (Cheng et al., 2000) and  $1.55125 \times 10^{-10} \text{ yr}^{-1}$  for  $^{238}\text{U}$  (Begemann et al., 2001). All ages are corrected for detrital  $^{230}\text{Th}$  using  $(^{238}\text{U}/^{232}\text{Th})_{\text{activity ratio}} = 0.9 \pm 0.45$  measured on clay of Villars cave. This correction was made thanks to ISOPLOT3 kindly provided by Kenneth Ludwig, Berkeley Geochronological center (Ludwig, 2003).

Sample	Situation (cm/top)	$\pm$ (cm)	$[^{238}\text{U}]$ (ng/g)	$\pm$	$\delta^{234}\text{U}$ (‰)	$\pm$	$(^{230}\text{Th}/^{238}\text{U})$ (Activity ratio)	$\pm$	$(^{230}\text{Th}/^{232}\text{Th})$ (Activity ratio)	$\pm$	Uncorr. age (ka)	$\pm$	Corr. age (ka)	$\pm$	Age err %	Laboratory
A	2.90	0.00	18.00	0.01	15.64	3.30	0.0983	0.0018	58.7	1.4	11.116	0.216	10.952	0.231	2.1	LSCE
<b>F1</b>	<b>3.65</b>	<b>0.25</b>	<b>34.36</b>	<b>0.02</b>	<b>45.79</b>	<b>2.77</b>	<b>0.0978</b>	<b>0.0018</b>	<b>14.7</b>	<b>0.3</b>	<b>10.713</b>	<b>0.207</b>	<b>10.082</b>	<b>0.377</b>	<b>3.7</b>	<b>GSI</b>
geotT	5.84	0.50	19.20	0.10	2.22	7.78	0.3157	0.0108	17.5	0.6	41.309	1.762	39.503	1.981	5.0	GEOTOP
<b>E1</b>	<b>5.90</b>	<b>0.30</b>	<b>18.90</b>	<b>0.01</b>	<b>3.89</b>	<b>2.03</b>	<b>0.2673</b>	<b>0.0064</b>	<b>14.0</b>	<b>0.3</b>	<b>33.801</b>	<b>0.958</b>	<b>31.894</b>	<b>1.358</b>	<b>4.3</b>	<b>GSI</b>
<b>D</b>	<b>10.95</b>	<b>0.65</b>	<b>35.15</b>	<b>0.21</b>	<b>2.51</b>	<b>31.79</b>	<b>0.3624</b>	<b>0.0181</b>	<b>7.8</b>	<b>0.4</b>	<b>48.970</b>	<b>3.725</b>	<b>44.256</b>	<b>4.358</b>	<b>9.8</b>	<b>GEOTOP</b>
<b>D1</b>	<b>11.30</b>	<b>0.30</b>	<b>32.65</b>	<b>0.02</b>	<b>0.25</b>	<b>1.81</b>	<b>0.3780</b>	<b>0.0037</b>	<b>5.9</b>	<b>0.1</b>	<b>51.825</b>	<b>0.670</b>	<b>45.239</b>	<b>3.466</b>	<b>7.7</b>	<b>GSI</b>
<b>C1</b>	<b>11.95</b>	<b>0.25</b>	<b>20.64</b>	<b>0.01</b>	<b>-16.15</b>	<b>2.73</b>	<b>0.3937</b>	<b>0.0089</b>	<b>5.6</b>	<b>0.1</b>	<b>55.895</b>	<b>1.664</b>	<b>48.522</b>	<b>4.203</b>	<b>8.7</b>	<b>GSI</b>
<b>A1</b>	<b>13.10</b>	<b>0.40</b>	<b>26.34</b>	<b>0.03</b>	<b>-3.40</b>	<b>3.04</b>	<b>0.5427</b>	<b>0.0093</b>	<b>14.0</b>	<b>7.8</b>	<b>85.939</b>	<b>2.284</b>	<b>81.006</b>	<b>3.417</b>	<b>4.2</b>	<b>GSI</b>
E	15.80	1.00	35.43	0.12	-3.31	6.51	0.6272	0.0240	12.4	0.5	108.444	7.245	103.276	7.718	7.5	GEOTOP
<b>F</b>	<b>23.75</b>	<b>0.75</b>	<b>40.03</b>	<b>0.19</b>	<b>1.47</b>	<b>10.34</b>	<b>0.5749</b>	<b>0.0078</b>	<b>57.8</b>	<b>0.8</b>	<b>93.157</b>	<b>2.633</b>	<b>92.167</b>	<b>2.672</b>	<b>2.9</b>	<b>GEOTOP</b>
Z	23.80	0.40	43.59	0.05	-17.97	2.40	0.5116	0.0042	108.4	1.0	80.590	1.044	80.110	1.072	1.3	GSI
<b>AI</b>	<b>45.40</b>	<b>0.50</b>	<b>73.60</b>	<b>0.06</b>	<b>3.89</b>	<b>2.89</b>	<b>0.6831</b>	<b>0.0034</b>	<b>126.0</b>	<b>0.7</b>	<b>124.446</b>	<b>1.380</b>	<b>123.910</b>	<b>1.405</b>	<b>1.1</b>	<b>GSI</b>
I	46.00	1.20	71.02	0.28	0.45	8.09	0.7107	0.0122	120.2	2.2	135.283	5.253	134.695	5.258	3.9	GEOTOP
AA	46.65	0.50	68.66	0.10	14.13	2.98	0.6977	0.0073	81.3	3.5	126.648	2.633	125.798	2.669	2.1	OU
Y	46.80	0.40	58.65	0.09	10.34	4.03	0.7903	0.0073	49.6	0.5	165.622	4.039	164.055	4.110	2.5	GSI
X	47.60	0.40	33.00	0.05	21.22	5.37	0.8017	0.0095	41.6	0.5	166.210	5.197	164.392	5.263	3.2	GSI
AB-2	47.90	0.50	41.18	0.08	41.81	4.61	0.7532	0.0066	60.9	2.5	138.202	2.794	137.016	2.849	2.1	OU
<b>J</b>	<b>49.50</b>	<b>1.00</b>	<b>53.09</b>	<b>0.20</b>	<b>24.76</b>	<b>8.60</b>	<b>0.7045</b>	<b>0.0274</b>	<b>61.0</b>	<b>2.6</b>	<b>126.068</b>	<b>9.464</b>	<b>124.954</b>	<b>9.477</b>	<b>7.6</b>	<b>GEOTOP</b>
AH	50.60	0.30	39.61	0.03	20.29	2.46	0.7557	0.0047	76.4	0.5	146.271	2.077	145.314	2.126	1.5	GSI
W	50.85	0.35	42.66	0.02	16.64	2.22	0.7060	0.0057	99.5	0.9	128.805	2.085	128.115	2.112	1.6	GSI
Q	50.95	0.45	43.75	0.21	28.51	9.72	0.7071	0.0200	182.1	5.3	125.943	7.142	125.572	7.143	5.7	GEOTOP
AJ	51.20	0.30	40.58	0.22	23.56	5.92	0.7281	0.0072	38.0	0.4	134.646	3.146	132.790	3.262	2.5	GEOTOP
AC	52.15	0.55	33.37	0.05	15.81	3.00	0.7624	0.0074	197.2	8.3	150.659	3.350	150.263	3.355	2.2	OU
AG	54.50	0.50	37.05	0.02	20.29	2.56	0.7536	0.0066	68.8	0.6	145.387	2.798	144.326	2.843	2.0	GSI
<b>Ksup</b>	<b>58.25</b>	<b>0.75</b>	<b>42.79</b>	<b>0.20</b>	<b>25.54</b>	<b>9.60</b>	<b>0.7089</b>	<b>0.0099</b>	<b>70.7</b>	<b>1.1</b>	<b>127.356</b>	<b>4.245</b>	<b>126.391</b>	<b>4.262</b>	<b>3.4</b>	<b>GEOTOP</b>
AD	58.70	0.30	49.55	0.09	29.88	4.16	0.7802	0.0073	64.9	2.7	152.896	3.490	151.686	3.538	2.3	OU
Kinf	58.75	0.65	31.72	0.02	16.64	3.61	0.7596	0.0115	128.6	2.1	149.163	4.982	148.590	4.989	3.4	GSI
AM	59.00	0.40	39.37	0.24	25.03	5.21	0.7312	0.0104	36.2	0.5	135.308	4.089	133.354	4.189	3.1	GEOTOP
<b>AE</b>	<b>59.50</b>	<b>0.30</b>	<b>50.25</b>	<b>0.21</b>	<b>87.30</b>	<b>26.19</b>	<b>0.7727</b>	<b>0.0168</b>	<b>296.0</b>	<b>16.0</b>	<b>131.900</b>	<b>8.831</b>	<b>131.664</b>	<b>8.826</b>	<b>6.7</b>	<b>OU</b>
AF	60.80	0.50	50.69	0.03	14.82	2.27	0.7641	0.0060	108.5	0.9	151.759	2.732	151.073	2.752	1.8	GSI
<b>geotS</b>	<b>61.00</b>	<b>0.07</b>	<b>47.63</b>	<b>0.33</b>	<b>10.42</b>	<b>7.48</b>	<b>0.7550</b>	<b>0.0093</b>	<b>70.4</b>	<b>0.9</b>	<b>149.535</b>	<b>4.832</b>	<b>148.482</b>	<b>4.853</b>	<b>3.3</b>	<b>GEOTOP</b>
R	62.20	0.04	41.56	0.21	-5.21	7.82	0.8102	0.0135	47.3	0.8	184.490	9.322	182.762	9.357	5.1	GEOTOP
S	62.50	0.30	41.45	0.05	7.35	2.56	0.8386	0.0086	46.9	0.5	194.183	5.753	192.416	5.821	3.0	GSI
T	63.00	0.30	44.11	0.03	9.40	3.07	0.8567	0.0057	54.9	0.4	204.841	4.575	203.305	4.637	2.3	GSI
<b>Lsup</b>	<b>63.50</b>	<b>0.40</b>	<b>38.82</b>	<b>0.14</b>	<b>10.88</b>	<b>10.11</b>	<b>0.7748</b>	<b>0.0143</b>	<b>34.0</b>	<b>0.6</b>	<b>158.050</b>	<b>7.786</b>	<b>155.795</b>	<b>7.848</b>	<b>5.0</b>	<b>GEOTOP</b>
<b>U</b>	<b>63.85</b>	<b>0.30</b>	<b>37.67</b>	<b>0.02</b>	<b>5.71</b>	<b>1.57</b>	<b>0.7817</b>	<b>0.0049</b>	<b>59.0</b>	<b>0.4</b>	<b>163.549</b>	<b>2.467</b>	<b>162.237</b>	<b>2.554</b>	<b>1.6</b>	<b>GSI</b>
<b>V</b>	<b>64.45</b>	<b>0.25</b>	<b>35.82</b>	<b>0.04</b>	<b>7.53</b>	<b>2.36</b>	<b>0.7897</b>	<b>0.0069</b>	<b>69.3</b>	<b>0.6</b>	<b>166.616</b>	<b>3.587</b>	<b>165.491</b>	<b>3.630</b>	<b>2.2</b>	<b>GSI</b>
AK	70.00	0.30	58.37	0.36	8.42	6.68	0.8008	0.0083	64.8	0.7	171.855	5.457	170.632	5.483	3.2	GEOTOP
<b>M</b>	<b>76.74</b>	<b>1.05</b>	<b>37.63</b>	<b>0.18</b>	<b>3.35</b>	<b>9.16</b>	<b>0.7935</b>	<b>0.0105</b>	<b>106.3</b>	<b>1.5</b>	<b>170.589</b>	<b>7.090</b>	<b>169.849</b>	<b>7.093</b>	<b>4.2</b>	<b>GEOTOP</b>
AL	80.00	0.30	47.88	0.30	3.32	5.01	0.8120	0.0091	72.7	0.8	180.626	5.892	179.518	5.915	3.3	GEOTOP
<b>B</b>	<b>97.70</b>	<b>0.00</b>	<b>32.00</b>	<b>0.02</b>	<b>9.03</b>	<b>2.20</b>	<b>0.8124</b>	<b>0.0052</b>	<b>130.2</b>	<b>1.3</b>	<b>177.692</b>	<b>3.060</b>	<b>177.080</b>	<b>3.074</b>	<b>1.7</b>	<b>LSCE</b>
<b>P</b>	<b>109.95</b>	<b>0.65</b>	<b>45.67</b>	<b>0.16</b>	<b>6.58</b>	<b>9.00</b>	<b>0.8110</b>	<b>0.0070</b>	<b>217.8</b>	<b>2.0</b>	<b>178.247</b>	<b>6.202</b>	<b>177.880</b>	<b>6.201</b>	<b>3.5</b>	<b>GEOTOP</b>

around 58.7 cm, Table 1 and Fig. 4) suggesting a potential “open-system” behaviour with respect to U. Optical microscope and scanning electron microscope (SEM) observations yielded no petrographic evidence for dissolution processes which could explain these concentration variations. Nevertheless, removal of U cannot be excluded on this basis alone, because these observations remain very local.

Concentration peaks of K, Na, and Zn associated with sharp U concentration variations, might lend support to the hypothesis of overestimated ages caused by detrital contamination as the main cause of too old ages. This appears unlikely, however, because  $^{230}\text{Th}/^{232}\text{Th}$  ratios are relatively high (36–296, Table 1) in this section. The observation that the largest peaks in trace element concentrations correlate with the first  $\delta^{18}\text{O}_c$  depletion (59.1 cm/top) suggests that they are related, possibly reflecting an episode of enhanced soil and epikarst flush following a long dry period. Thus the trace elements peak does not necessarily imply that flowstone leaching re-mobilized uranium. This hypothesis cannot be ruled out, however, since the typical mass of U-series samples is significantly larger than that of trace elements samples (on the order of 1 g for the former, versus 30–60  $\mu\text{g}$  for the latter): one cannot rule out

that a dilution effect is hiding a large but localized detrital contamination affecting the U-series analysis.

In view of these results, it remains challenging to prove or disprove either hypothesis (detrital contamination versus U leaching). However, both cases would result in overestimated ages, and we accordingly based our age model on linear interpolation between the youngest dated points for each calcite layer, which yields a chronology consistent with respect to the other major absolutely dated records in this area (i.e. Soreq Cave and Corchia Cave record, Fig. 5).

We used the same strategy as above (linear interpolation between the youngest dated points for each calcite layer) between 6 and 5 cm/top (U–Th–geoT and U–Th–E1, Fig. 5). Finally, from 15 to 24 cm/top, we considered the more logical solution. All dated points used for the age model are shown in bold in Table 1.

The discontinuity d63.5 is marked both by a clay-rich layer and a change of petrography (from white porous laminated to dark compact calcite, Figs. 2 and 5); this discontinuity corresponds to the appearance of a new generation of crystals. These observations, along with the sharp change in the youngest U–Th dates across that transition, suggest the occurrence of a hiatus between ~156 and

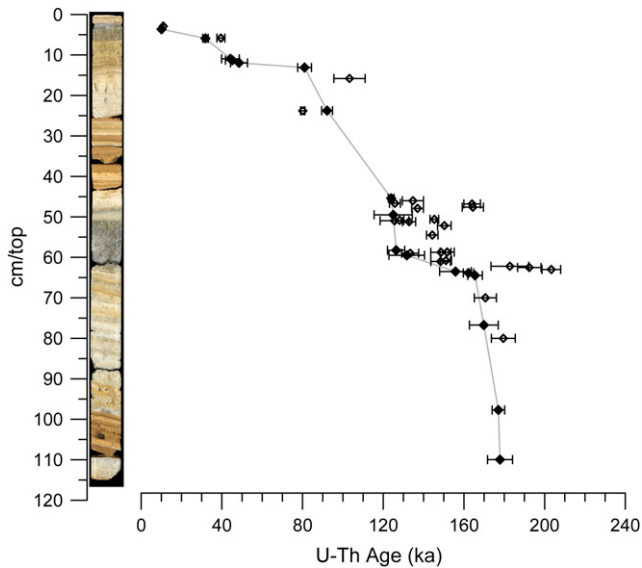


Fig. 5. Vil-car-1 sample growth curve. The grey line in between the full symbols represents the age model chosen. Empty symbols are the others U–Th ages get on the core ( $2\sigma$  error shown).

148 ka. Such an interruption of flowstone growth might be linked to the cold and dry climate during mid-MIS6 (Table 1, Figs. 1, 5 and 6). This interpretation appears to be supported by very slow growth rates on both sides of this hiatus (respectively  $\sim 0.5$  and  $\sim 2$  mm/ka immediately before and after the discontinuity). From  $126.4 \pm 4.3$  ka onwards, the growth rate increases to  $\sim 6$  cm/ka (Fig. 5).

We must acknowledge the imprecision in our age model, which in some sections suffers from significant uncertainties. Nevertheless, the Vil-car-1 profiles of  $\delta^{18}\text{O}_c$  and  $\delta^{13}\text{C}_c$  plotted against the age model are very consistent with isotopic records obtained from other Villars speleothems for the period of 50–0 ka (Supplementary material, figure A). Additionally, as shown in Fig. 6, the older part of the Vil-car-1 record is similarly consistent with the composite record from Soreq cave (Bar-Matthews et al., 2003) and with those from Corchia cave (Drysdale et al., 2005, 2009). Based on this external consistency, we conclude that the flowstone section from 63.5 to 42 cm/top was deposited between 148.3 and 122.7 ka, and that the prominent negative  $\delta^{18}\text{O}_c$  peak corresponds to the Last Interglacial period. In the rest of this study, we focus on understanding which factors may have driven these large variations in  $\delta^{18}\text{O}_c$ .

#### 4.4. Isotopic composition of fluid inclusion water

Samples for fluid inclusion analysis were collected from calcite layers deposited before, during, and after Termination II (Table 2; Figs. 7 and 8). Importantly, the oxygen isotope composition of fluid inclusions ( $\delta^{18}\text{O}_w$ ) remains constant within  $\sim 1\text{‰}$  even across the abrupt 4–5‰ decrease in  $\delta^{18}\text{O}_c$  (Table 2, Fig. 8). This observation was consistently reproduced in analyses performed in two different laboratories (VU and UI). Although the absolute values suffer from systematic laboratory bias ( $\delta^{18}\text{O}_w$  and  $\delta\text{D}_w$  values measured at VU come out as  $\sim 1\text{‰}$  and  $\sim 3\text{‰}$  heavier, respectively, than those from UI, as reported in Table 2), the absence of a detectable change in the  $\delta^{18}\text{O}_w$  values of drip waters across TII can be robustly established.

### 5. Discussion: the Vil-car-1 oxygen isotopic shift

In previous speleothem records from Villars Cave, the amplitude of  $\delta^{18}\text{O}_c$  variations remained limited, in contrast to  $\delta^{13}\text{C}_c$  profiles, displaying striking climatic features (Genty et al., 2003, 2005;

Wainer et al., 2009). This 5‰ amplitude of  $\delta^{18}\text{O}_c$  variation recorded by Vil-car-1 is unusually large but previous records from this cave only extended back as far as  $\sim 80$  ka, and thus covered neither Termination II nor the Last Interglacial. It is thus important to understand the physical causes for the observed depletion in  $\delta^{18}\text{O}_c$  at the time of Termination II, and in particular to distinguish between “regional” factors such as cave temperature and drip water composition, and “micro-environmental” factors such as disequilibrium precipitation of calcite at the surface of the flowstone. Most of the following discussion will thus focus on the identification and quantification of these two potential causes for the significant  $\delta^{18}\text{O}_c$  depletion across TII *sensu lato*.

According to studies of modern north European stalagmites, 80–90% from the speleothem carbon comes from the soil biogenic  $\text{CO}_2$  and 10–20% from the calcareous hostrock (Genty and Massault, 1997, 1999; Vogel and Kronfeld, 1997; Genty et al., 2001). The  $\delta^{13}\text{C}_c$  was interpreted as closely linked with the density of the vegetation cover and microbial activity above the cave. The denser the vegetation enhancing the part of biogenic  $\text{CO}_2$ , the more negative the  $\delta^{13}\text{C}_c$  values would be. Usually, the  $\delta^{18}\text{O}_c$  variations in Villars during the last 80 ka are within 1‰ which makes its interpretation difficult (Genty et al., 2003, 2005; Wainer et al., 2009). The Vil-car-1  $\delta^{18}\text{O}_c$  profile offers the opportunity to study the factors involved in oxygen isotopic variations in Villars Cave at the time of the Termination II. As a consequence, we will focus our interest on Vil-car-1  $\delta^{18}\text{O}_c$  in the section located between 63.5 and 42 cm/top. Other parts will be studied in more details in other studies.

It should be noted that the large  $\delta^{18}\text{O}_c$  depletion ( $-5\text{‰}$ ) recorded in Vil-car-1 across Termination II is synchronous, within age model errors, to the largest isotopic variations recorded in both Corchia cave and Soreq cave (Bar-Matthews et al., 2003; Drysdale et al., 2005, 2007, 2009) suggesting that it does not reflect a purely local effect. Furthermore, based on the similarity between the Vil-car-1 and Soreq cave records (Fig. 6), it is tempting to attribute both  $\delta^{18}\text{O}_c$  depletions across TII to similar causative mechanisms, i.e., to the combination of (a) a change of source vapor  $\delta^{18}\text{O}$ , (b) a temperature increase, and (c) an increase in the amount of meteoric precipitation (Matthews et al., 2000; Bar-Matthews et al., 2003; McGarry et al., 2004).

The two sites, however, are separated by more than 3000 km and are located in very different climatic settings. In contrast to the Soreq site, the oxygen isotopic composition of modern rainfall at Villars is not inversely correlated with rainfall amount but rather shows a correlation with the seasonal temperatures (Bar-Matthews et al., 1999; Genty, 2008). Rainfall reconstructions based on pollen records from the Velay lakes ( $44^\circ 54' \text{N}$ ,  $3^\circ 47' \text{E}$ , 1200 masl, Fig. 1) indicate a  $\sim 400$  mm increase in precipitation, and an associated increase in January temperature of  $\sim 20^\circ \text{C}$  contemporaneous to the Vil-car-1  $\delta^{18}\text{O}_c$  depletion (Fig. 6; (Beaulieu et al., 1991; Cheddadi et al., 1998, 2005)). However, the Velay record yields similar rainfall increases at the transitions MIS5b/5a and MIS2/MIS1, but which did not result in any significantly discernible  $\delta^{18}\text{O}_c$  response in the Vil-car-1 record (Fig. 6). Moreover, data from the closest IAEA stations do not show any significant correlation between rainfall amount and rain  $\delta^{18}\text{O}$  composition (Brest, Orléans, Thonon GNIP IAEA data). This lack of correlation between pluviometry and rainfall  $\delta^{18}\text{O}$  values might be explained by the geographical location of Villars cave close to the Atlantic Ocean where the amount effect is less likely pronounced than for more continental settings. It is thus unlikely that the amount effect is the controlling factor of the Vil-car-1  $\delta^{18}\text{O}_c$  shift at Termination II.

This conclusion is consistent with fluid inclusion results, which indicate that  $\delta^{18}\text{O}_w$  remained constant over TII (Fig. 7). This implies that the  $\delta^{18}\text{O}_c$  shift must be attributed to other factors such as cave

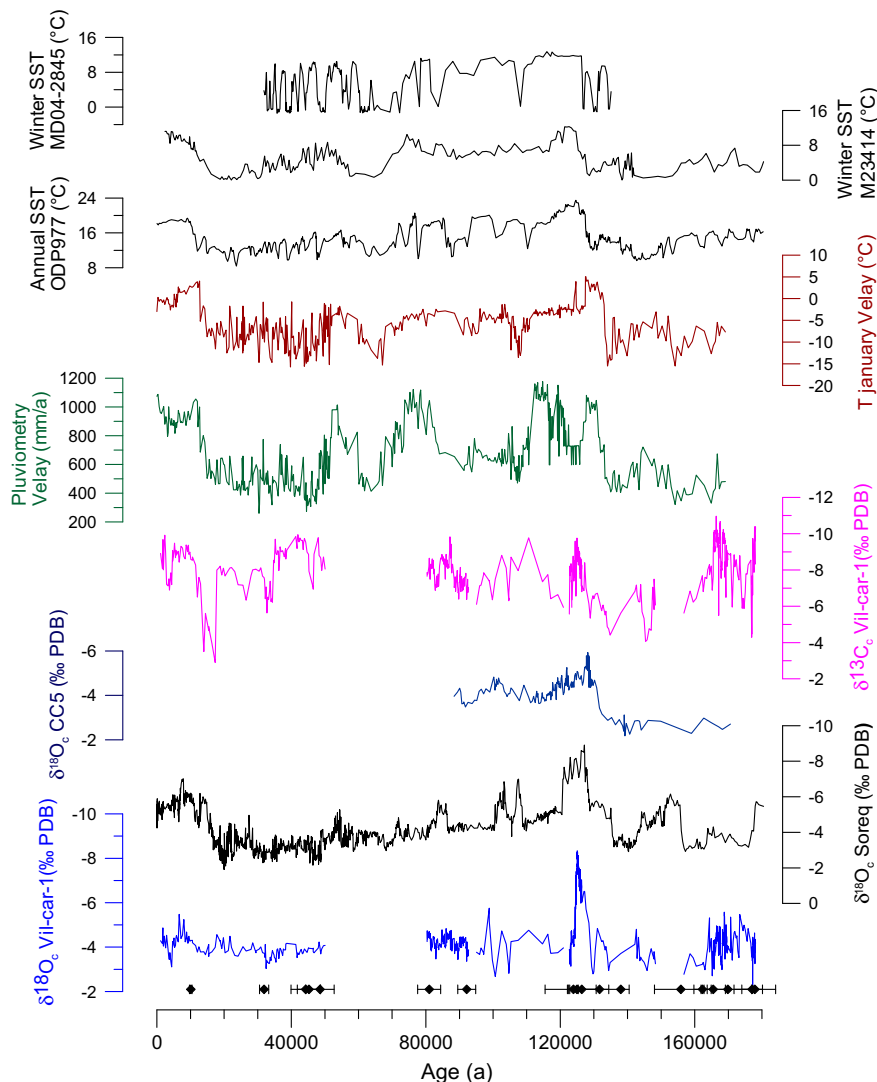


**Fig. 6.** Comparison between Vil-car-1  $\delta^{18}\text{O}_c$  and  $\delta^{13}\text{C}_c$  with Soreq  $\delta^{18}\text{O}_c$  (modified from Bar-Matthews et al., 2003) Corchia Cave CC5  $\delta^{18}\text{O}_c$  (Drysdale et al., 2005) and Velay plateau rainfall annual quantity and January temperature estimations (Beaulieu et al., 1991; Cheddadi et al., 2005), mean annual SST temperature calculated thanks to the  $\text{U}_{77}$  alkenones index ODP977 core (Martrat et al., 2004), winter SST deduced from foraminifers assemblages of MD04-2845 (Bay of Biscay, Sánchez Goñi et al., 2008) and M23414 Northern Atlantic (Kandiano et al., 2004) marine cores.

temperature rise and possibly variable amounts of out-of-equilibrium precipitation.

## 5.1. Amplitude of temperature increase across Termination II

### 5.1.1. Did Vil-car-1 calcite precipitate in isotopic equilibrium?

#### a) Classical equilibrium tests

Although the Hendy tests described in Section 4.1.1 yield no clear evidence for out-of-equilibrium precipitation in four out of the five tested Vil-car-1 laminae (Fig. 3), this does not constitute reliable evidence for thermodynamic equilibrium, for several reasons. Strictly speaking, the Hendy test can only provide evidence of spatially variable disequilibrium fractionation. Although one might argue that kinetic isotope fractionation effects near the apex of a stalagmite would likely display detectable lateral variations, that assumption is far less likely to hold true at the scale of a flow area several meters wide, but only sampled within the diameter of the core (7.5 cm), half meter

away from the flowstone's main water supply. Additionally, individual laminae proved too subtle and too thin to be separately subsampled in a strict manner. For these reasons, we do not entirely trust this test and suspect that the Vil-car-1 record may partly reflect out-of-equilibrium deposition due to kinetic isotope fractionation effects.

On the other hand, Vil-car-1 profiles of  $\delta^{18}\text{O}_c$  and  $\delta^{13}\text{C}_c$  for the last ~80 ka are quantitatively consistent with coeval stalagmite records from elsewhere in the same cave (Supplementary material fig. A), and a such internal consistency might be indicative of equilibrium precipitation (Dorale et al., 2002; Wang et al., 2008). However, there is unambiguous and widespread evidence that modern calcite precipitates out of equilibrium in the Villars cave: Genty (2008) measured the isotopic compositions of modern drip water and of recent calcite samples, some of which were collected only a few meters from the Vil-car-1 flowstone. Temperatures computed from these measurements by means of various equilibrium fractionation equations (Kim and O'Neil, 1997; O'Neil et al., 1969; Craig, 1965 equations) differed significantly (4–5 °C discrepancy) from the modern temperature

**Table 2**

Villars cave modern drip water and Vil-car-1 fluid inclusion oxygen and hydrogen isotopic composition. Modern drip water analyses were made by (Genty et al., 2008 and Genty et al., 2010). The modern drip water isotopic compositions given in this table correspond to the mean of the n samples collected between 2000 and 2007. For fluid inclusion sample the number in brackets is the serial number.

Sample ID	cm/top	U-Th age (ka)	$\delta^{18}\text{O}_{\text{w}/\text{o}} \text{‰ SMOW}$	$\pm 1\sigma$	$\delta^2\text{H}_{\text{w}/\text{o}} \text{‰ SMOW}$	$\pm 1\sigma$
<i>Modern drip water</i>						
Lower galleries Stt 1A			-6.4 (n = 26)	0.05	-39.4 (n = 21)	1.1
Lower galleries-Stt 1B			-6.4 (n = 31)	0.1	-39.4 (n = 23)	0.7
Upper galleries-Stt10A			-6.2 (n = 30)	0.2	-37.2 (n = 25)	2.0
Upper galleries-Stt 10B			-6.2 (n = 22)	0.1	-37.3 (n = 18)	1.3
<i>Fluid inclusions VU</i>						
Vil-car-1-FI-K(3)	64.9	165.6	-6.2 (n = 2)	0.5	-49.0 (n = 2)	1.5
Vil-car-1-FI-A(1)	62.8	145.7	-6.4 (n = 2)	0.5	-47.3 (n = 2)	1.5
Vil-car-1-FI-H(3)	60.8	137.9	-6.2 (n = 2)	0.5	-49.0 (n = 2)	1.5
Vil-car-1-FI-D(2)	60.8	137.9	-6.8 (n = 1)	0.5	-43.1 (n = 1)	1.5
Vil-car-1-FI-C(2)	59.0	129.6	-6.2 (n = 1)	0.5	-42.7 (n = 1)	1.5
Vil-car-1-FI-J(3)	56.0	126.0	-5.7 (n = 1)	0.5	-44.2 (n = 1)	1.5
Vil-car-1-FI-E(2)	54.5	125.8			-41.3 (n = 2)	1.5
Vil-car-1-FI-G(3)	50.8	125.2	-6.0 (n = 1)	0.5	-43.1 (n = 1)	1.5
Vil-car-1-FI-F(2)	50.6	125.1	-7.1 (n = 1)	0.5	-45.9 (n = 1)	1.5
Vil-car-1-FI-B(1)	50.6	125.1	-6.2 (n = 2)	0.5	-48.1 (n = 2)	1.5
Vil-car-1-FI-I(3)	49.5	125.0	-7.0 (n = 4)	0.5	-55.0 (n = 4)	1.5
Average			-6.4		-46.2	
Standard deviation			0.4		4.0	
<i>Fluid inclusions IU</i>						
Vil-car1-FI-A	62.8	145.7	-7.1 (n = 2)	0.5	-47.9 (n = 2)	1.5
Vil-car1-FI-H	60.8	137.9	-7.4 (n = 2)	0.5	-46.8 (n = 2)	1.5
Vil-car1-FI-N	57	126.2	-7.3 (n = 1)	0.5	-52.4 (n = 1)	1.5
Vil-car1-FI-G	50.8	125.2	-7.1 (n = 2)	0.5	-48.9 (n = 1)	1.5
Average			-7.2		-49.0	
Standard deviation			0.1		2.4	

directly observed at this site. This implies that isotopic equilibrium is not attained during modern calcite precipitation, even in this part of the cave despite its high humidity, the presence of pools, and absence of any significant air flow. Good agreement between isotopic profiles from different Villars speleothems should thus not be interpreted as evidence for equilibrium precipitation, but rather that they experience similar amounts of kinetic isotope fractionation (within  $\sim 0.25\text{‰}$ , based on the observations of (Genty, 2008)).

b) Comparisons of calcite  $\delta^{18}\text{O}_{\text{c}}$  values versus fluid inclusion  $\delta^{18}\text{O}_{\text{w}}$ .

An alternative test of thermodynamic equilibrium was applied to the core section between 63.5 cm and 49 cm/top, by comparing the  $\delta^{18}\text{O}$  values of fluid inclusions with those of the surrounding calcitic matrix. Assuming (a) that the inclusions and the

surrounding calcite are coeval, and (b) that the oxygen isotope composition of trapped fluids did not vary over time, one can use published water/calcite equilibrium calibrations to reconstruct cave paleotemperatures, and assess whether these temperature predictions are physically realistic.

A caveat must be kept in mind: as previously noted (e.g. (Verheyden, 2001; Genty, 2008)), the numeric results of such computations are strongly dependent on which published equilibrium relationship is selected (McCrea, 1950; Epstein et al., 1953; Craig, 1965; O'Neil et al., 1969; Friedman and O'Neil, 1977; Kim and O'Neil, 1997; Coplen, 2007). Although in Table 3 we compare reconstructed temperatures derived from several of these calibrations, in Fig. 8 and in the following discussion we mainly focus on the Kim and O'Neil (1997) relationship, because (a) it is applicable to abiotic carbonates and (b) the calcite precipitation experiments were designed to minimize potential kinetic effects and fit well with the studied environment.

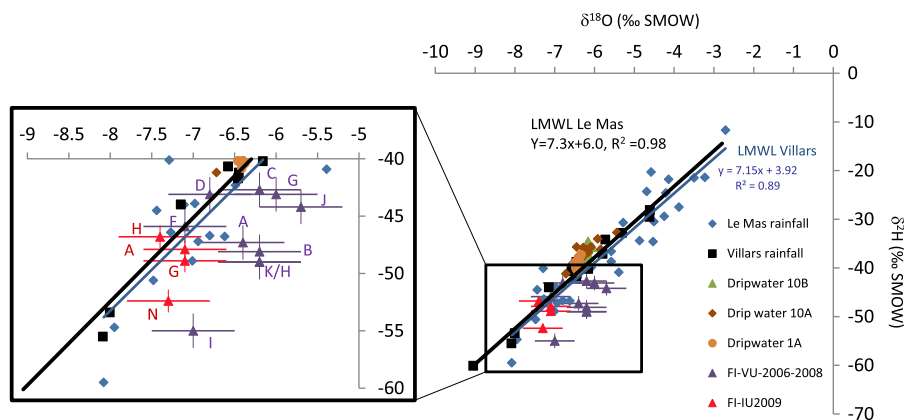


**Fig. 7.** Modern Rainfall and fluid inclusions  $\delta\text{D}$  vs  $\delta^{18}\text{O}$ . The local meteoric water line is drawn based on Villars and Le Mas (70 km SW from Villars) rainfall water composition (Genty et al., 2005, 2008, 2010).

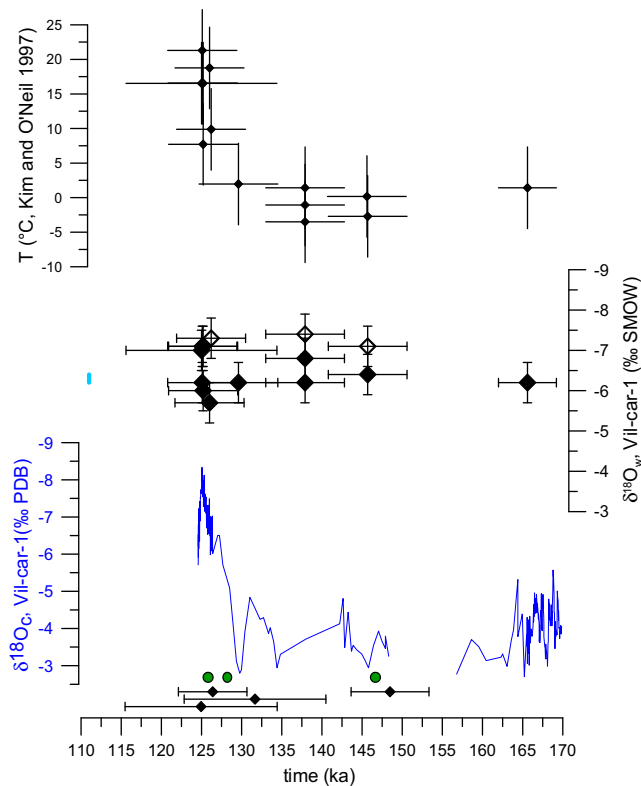


**Fig. 8.** Oxygen isotopic composition of both Vil-car-1 calcite, fluid inclusions  $\delta^{18}\text{O}_w$  and equilibrium temperature deduced from the Kim and O'Neil formula ( $1\sigma$  error shown). Black diamonds at the bottom indicate the dated points used in the age model on this part of the core. Mean modern drip water composition is indicated by light blue rectangle on the left hand side. Empty diamonds represents the IU data and full ones the VU data. Green circles indicate where the clumped isotope samples were collected. (For interpretation of the references to colour in this figure legend, the reader is referred to the web version of this article.)

Although several of the reconstructed temperatures for Late MIS6 appear to be negative, they are not statistically below freezing temperatures due to the rather large uncertainties associated with fluid inclusion spectrometry. Regardless of the preferred equilibrium calibration, the total thermal amplitude from Late MIS6 to the

MIS5  $\delta^{18}\text{O}_c$  “optimum” is on the order of  $+25^\circ\text{C}$ . Although it is generally expected that TII was characterized by a greater thermal amplitude (e.g. Vimeux et al., 2002; NorthGRIPmembers, 2004; Köhl and Litt, 2007), this is more than twice the amount of warming estimated across Termination I (e.g. Wu et al., 2007).

Independent, quantified temperatures estimates for Termination II itself are scarce in this continental area. Based on pollen data from the nearby Velay plateau lakes cores the maximum thermal amplitude of TII is about  $18\text{--}20^\circ\text{C}$  (Fig. 6, (Beaulieu et al., 1991; Cheddadi et al., 2005)). Alternatively, the inverse mode of the Biome4 vegetation model constrained with pollen data and  $\delta^{13}\text{C}$  of the Grande Pile core GPXXI ( $\sim 650$  km ENE from Villars, 330 masl) yield a temperature rise of at least  $13.6 \pm 5.3^\circ\text{C}$  (Rousseau et al., 2006). In light of these independent constrains, the  $+25^\circ\text{C}$  temperature rise in Villars cave reconstructed above appears significantly overestimated, even taking into account the large uncertainties inherent to all these methods.

To summarize, oxygen isotope measurements of modern material and fluid inclusion analyses both imply that calcite within and around Vil-car-1 did not precipitate at thermodynamic equilibrium, and it appears likely that the corresponding isotopic record is affected by significant amounts of kinetic fractionation. This is further supported by the observations of Daëron et al. (submitted for publication) from a speleothem calibration study of “clumped isotopes” (see next section for more details).

### 5.1.2. Temperature rise from end of MIS6 to Last Interglacial optimum estimated from clumped isotope and fluid inclusion $\delta^{18}\text{O}$ measurements

In this section we discuss how our fluid inclusion data may be combined with independently reported “clumped isotope” measurements from the same core, in an attempt to quantitatively correct for kinetic isotope fractionations using the method described by Guo et al. (submitted for publication).

#### a) “Clumped isotopes” and speleothems

Clumped isotope thermometry offers an alternative method to estimate carbonate paleotemperatures. It is based on precise measurements of the abundances of multiply substituted isotopologues of the carbonate ion, such as  $(^{13}\text{C}^{18}\text{O}^{16}\text{O}_2)^{2-}$ , and does not require independent knowledge of the  $\delta^{18}\text{O}$  of water in the precipitating solution (Ghosh et al., 2006; Eiler, 2007). The crystallization temperature of carbonates formed at thermodynamic

**Table 3**

Theoretical paleo-temperature calculations based on calcite and fluid inclusions oxygen isotopic results. The theoretical equilibrium temperature uncertainties account for (a)  $\delta^{18}\text{O}_w$  0.5‰ uncertainty and (b) variability of the  $\delta^{18}\text{O}_c$  values over the sample thickness collected for fluid inclusion analyses. (Craig (1965):  $T(^{\circ}\text{C}) = 16.9 - 4.2 * (\delta^{18}\text{O}_c - \delta^{18}\text{O}_w) + 0.13(\delta^{18}\text{O}_c - \delta^{18}\text{O}_w)^2$ ; (PDB for  $\delta^{18}\text{O}_c$ , SMOW for  $\delta^{18}\text{O}_w$ ). Friedman and O'Neil (1977):  $T(^{\circ}\text{C}) = \sqrt{(2780000 / ((\delta^{18}\text{O}_c - \delta^{18}\text{O}_w) - 2.89) - 273.15)}$ ; (SMOW for  $\delta^{18}\text{O}_c$ , SMOW for  $\delta^{18}\text{O}_w$ ). Kim and O'Neil, (1997):  $T(^{\circ}\text{C}) = 18.03 \times 1000 / ((\delta^{18}\text{O}_c - \delta^{18}\text{O}_w) + 32.42) - 273.15$  (SMOW for  $\delta^{18}\text{O}_c$ , SMOW for  $\delta^{18}\text{O}_w$ ).

Sample	Depth	U–Th age	Milestone on the $\delta^{18}\text{O}_c$ Curve	$\delta^{18}\text{O}_c$	$\delta^{18}\text{O}_{\text{FI}}$	Theoretical temperature ( $^{\circ}\text{C}$ )		
						Craig, 1965	Friedman et O'Neil, 1977	Kim and O'Neil, 1997
	cm/top	(ka)		‰ VPDB	‰ VSMOW	$\pm 4.9$	$\pm 5.4$	$\pm 5.9$
Vil-car-1-FI-K(VU)	64.9	165.6	Early MIS6	-3.7	-6.2	7.2	4.2	1.4
Vil-car-1-FI-A(IU)	62.8	145.7	Late MIS6	-3.6	-7.1	3.8	0.4	-2.7
Vil-car-1-FI-A(VU)	62.8	145.6	Late MIS6	-3.6	-6.4	6.2	3.1	0.2
Vil-car-1-FI-H(VU)	60.8	137.9	Late MIS6	-3.7	-6.2	7.2	4.2	1.4
Vil-car-1-FI-H(IU)	60.8	137.9	Late MIS6	-3.7	-7.4	3.1	-0.3	-3.5
Vil-car-1-FI-D(VU)	60.8	137.9	Late MIS6	-3.7	-6.8	5.1	1.9	-1.1
Vil-car-1-FI-C(VU)	59	129.6	TII reversal	-3.8	-6.2	7.7	4.7	2.0
Vil-car-1-FI-N(IU)	57	126.2	LI plateau	-6.7	-7.3	14.3	12.1	9.9
Vil-car-1-FI-J(VU)	56	126	LI plateau	-7.0	-5.7	22.6	20.5	18.8
Vil-car-1-FI-G(VU)	50.8	125.2	LI Optimum	-6.0	-7.1	12.4	10.0	7.7
Vil-car-1-FI-G(IU)	50.8	125.2	LI Optimum	-7.9	-7.1	20.3	18.4	16.6
Vil-car-1-FI-F(VU)	50.6	125.1	LI Optimum	-7.9	-7.1	20.3	18.4	16.6
Vil-car-1-FI-B(VU)	50.6	125.1	LI Optimum	-8.00	-6.20	24.9	23.0	21.3
Vil-car-1-FI-I(VU)	49.5	125	LI	-7.80	-7.00	20.3	18.4	16.5

equilibrium can thus be directly derived from the measurement of  $\Delta_{47}$ , a variable describing the degree of isotopic “clumping” in  $\text{CO}_2$  evolved from carbonate samples. Clumped-isotope thermometry, if applied to speleothems, would potentially allow independent reconstructions of T and seepage water  $\delta^{18}\text{O}$ . Early investigations, however, have shown that  $\Delta_{47}$  values of modern speleothems formed under a wide range of environmental parameters are significantly less than expected for carbonate precipitating under equilibrium conditions (Affek et al., 2008; Daëron et al., submitted for publication). These systematic  $\Delta_{47}$  offsets likely result from kinetic isotope fractionation (KIF) caused by rapid degassing and crystallization reactions (Guo et al., 2008; Guo et al., submitted for publication).

#### b) Application to Vil-car-1

As part of a broader calibration study of  $\Delta_{47}$  in speleothems (cf supplementary material B for the methods and materials used in that study), Daëron et al. (submitted for publication) reported the clumped-isotope compositions of four samples from Vil-car-1, located respectively at 50.8, 58.6, 63.0, and 65.1 cm/top (Fig. 8). They observed that all Vil-car-1 temperatures computed from  $\Delta_{47}$  assuming equilibrium precipitation, including those for the glacial sample, consistently come out 9 to 20 °C warmer than modern cave temperatures. These unreasonably high temperatures are qualitatively consistent with modern clumped isotopes data from Villars cave (Daëron et al., submitted for publication), providing additional evidence for out-of-equilibrium precipitation. Faced with a similar problem, Affek et al. (2008) used the modern  $\Delta_{47}$  offset (i.e. the difference between the measured  $\Delta_{47}$  value and the expected equilibrium value for one modern speleothem) to correct for KIF in clumped-isotope measurement of fossil speleothems from the same cave, and the resulting paleotemperatures are consistent with Eastern Mediterranean sea-surface temperatures estimated using alkenone unsaturation ratios. The same method cannot be applied to Vil-car-1, however, because the clumped-isotope results of Daëron et al. provide unambiguous evidence that the core experienced large variations in the amplitude of KIF effects over time: correcting the Vil-car-1  $\Delta_{47}$  measurements by a fixed offset would inevitably yield an unrealistic thermal history, with temperature estimates for MIS6 significantly warmer than for the Last Interglacial.

An alternative method, proposed by Guo et al. (submitted for publication), describes how clumped-isotope data can be combined with fluid inclusion data to correct for KIF effects in speleothems and thus reconstruct absolute paleotemperatures. This requires estimating the correlation between  $\Delta_{47}$  effects and  $\delta^{18}\text{O}$  effects. In the case of Villars cave, Guo et al. used the four local, modern measurements of isotopic disequilibria described by Daëron et al. (submitted for publication) to estimate the average direction of the modern KIF vector in a 2D space defined by  $\Delta_{47}$  and  $1000\ln(\alpha)$ , where  $\alpha$  is the  $^{18}\text{O}$  fractionation factor between carbonate and water (Fig. 9). The two key assumptions behind this method are: (1) that, although the amplitude of KIF offsets affecting  $\Delta_{47}$  and  $\delta^{18}\text{O}$  may vary significantly over time, the relative balance between these two fractionation effects remains within certain limits, as implied by the strong correlation observed in modern speleothems worldwide (Fig. 4 in Daëron et al., submitted for publication); (2) that these limits may be reasonably well estimated by compiling modern observations, so that the correlation between  $\Delta_{47}$  and  $\delta^{18}\text{O}$  offsets is characterized by its mean value and its standard deviation, both observed within the same cave setting as Vil-car-1.

Only three of the four clumped-isotope samples reported by Daëron et al. (submitted for publication) are bracketed by our fluid

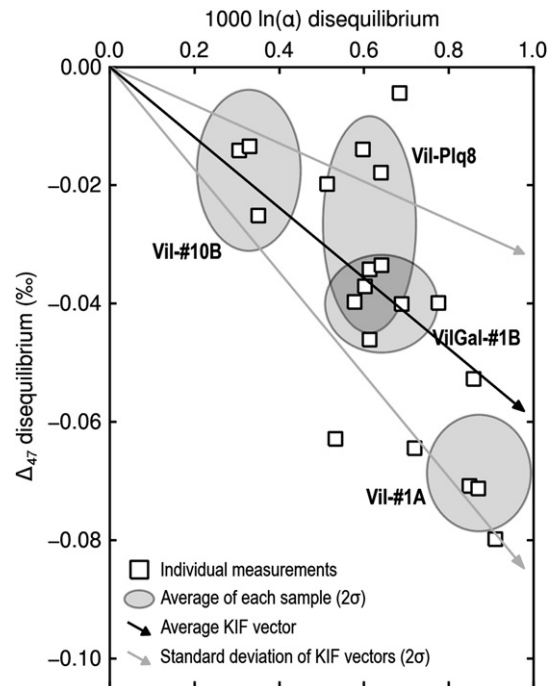
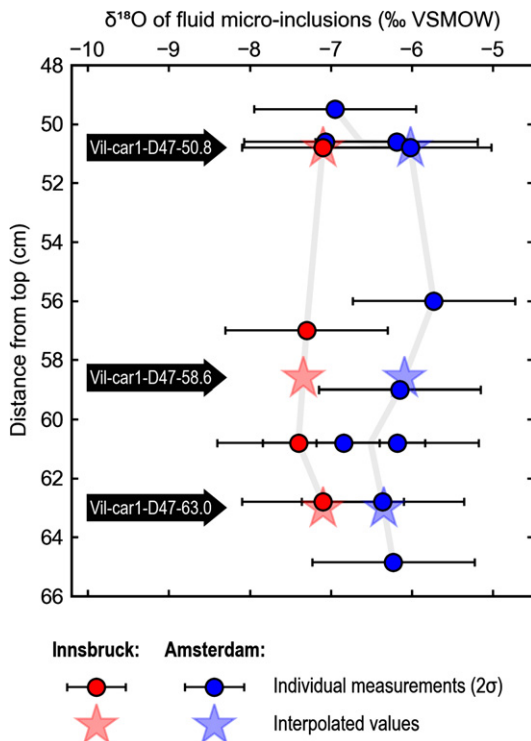


Fig. 9.  $\Delta_{47}$  offsets (relative to equilibrium values) vs  $1000\ln(\alpha)$  offsets for modern Villars cave calcite deposit. Open squares correspond to replicate analyses, and are indicative of analytical precision limits and sample inhomogeneities. Grey ellipses correspond to  $2\sigma$  confidence limits of the replicates for each different speleothem. The average slope is computed using sample means, not analytical replicates. Data from (Daëron et al., submitted for publication).

inclusion data (Fig. 10). These are Vil-car-1- $\Delta_{47}$ -63.0,  $-58.6$ , and  $-50.8$ , respectively corresponding to the Late MIS6, Termination II and MIS-5 optimum. Because of current analytical requirements, individual samples for FI analysis are typically 100 times larger than  $\Delta_{47}$  samples. Each FI measurement thus corresponds to a time-averaged value which is expected to display smaller short-term variations. For this reason, we selected to combine both data sets by interpolating FI  $\delta^{18}\text{O}_w$  values to the respective depths of the three  $\Delta_{47}$  samples (Fig. 10). Although this solution is not entirely satisfactory, FI and  $\Delta_{47}$  samples are in close proximity for 5 out of the 6 relevant data points (3 layers and 2 laboratories). Nevertheless, future studies would benefit from a protocol designed to successively perform both types of measurements on the same sample material. Because of the systematic offset between FI results from the Innsbruck and Amsterdam labs, we used data from both labs independently, compared the results, and estimated a posteriori how paleo-temperature estimates might be affected by these FI laboratory bias.

Each of the three samples may then be plotted on a graph of  $\Delta_{47}$  versus  $1000\ln(\alpha)$ , the latter being derived from the  $\delta^{18}\text{O}$  compositions of the carbonate material and of fluid inclusions (Fig. 11). In this 2D space, carbonate precipitated at thermodynamic equilibrium would plot along the “equilibrium line”, defined by the calibration functions of Kim and O’Neil (1997) and Ghosh et al. (2006). This is clearly not the case for the three Vil-car-1 samples, which all plot below the equilibrium line. Assuming, as stated above, that each sample was offset from its T-dependent location along the equilibrium line along a KIF vector whose length is a priori unknown and whose slope may vary through time according to the statistical distribution observed in modern Villars speleothems (Fig. 9), one may geometrically project each sample on the equilibrium line, thus estimating a KIF-corrected paleo-temperature of crystallization (Guo et al., submitted for publication).



**Fig. 10.** Relative positions of clumped isotope sampling locations (black arrows) and fluid inclusion data (red and blue markers). The stars correspond to the interpolated value deduced from bracketing measurements, at the exact depth of a clumped isotope measurement. (For interpretation of the references to colour in this figure legend, the reader is referred to the web version of this article).

Temperature uncertainties in Fig. 11 account for: (a) external precision limits on  $\Delta_{47}$ ; (b) a conservatively estimated uncertainty of 0.5‰ for fluid inclusion  $\delta^{18}\text{O}$  values; (c) the standard deviation observed in the slope of modern KIF vectors. Note that we do not assume that the KIF vector retains strictly the same slope through time: as stated above, that slope is allowed to vary within the limits estimated using modern observations. In spite of the incorporation of these significant sources of uncertainty, the formal standard error on temperature does not exceed 2 °C, which is not significantly worse than existing continental temperature reconstructions from other methods. Moreover, the dominant component in the variance of our T estimates is the uncertainty in the  $\delta^{18}\text{O}_w$ , which accounts for 80–85% of total variance (depending of which laboratory's FI data is used), to be compared with 11–16% from the KIF correlation and only 4–5% from  $\Delta_{47}$  uncertainties. Future attempts at this kind of “speleo-thermometry” may likely benefit from improved precision/accuracy in the oxygen spectrometry of fluid micro-inclusions.

The corrected fluid inclusion-clumped isotope temperatures range between 5.8 or 8.1 °C ( $\pm 1.9$  °C at  $1\sigma$ ) at late MIS6 to 19 or 22.7 ( $\pm 1.9$  °C at  $1\sigma$ ) for the MIS5 optimum (temperatures from UI and VU fluid inclusions data, respectively; uncertainties are given at  $2\sigma$ -level in Fig. 11). Using data from VU yields reconstructed temperatures warmer by 2.4–4.2 °C than those derived from the Innsbruck laboratory. We suspect that this is the consequence of a systematic bias in the VU fluid inclusion measurements, because the resulting  $\delta^{18}\text{O}$  and  $\delta\text{D}$  values are generally less consistent with the modern local meteoric water line, than the UI data (Fig. 7). Reliably estimating absolute cave paleotemperatures will thus require improving our understanding of (and ability to correct for) inter-laboratory differences in fluid inclusion analysis, which is the focus of an ongoing inter-laboratory calibration effort.

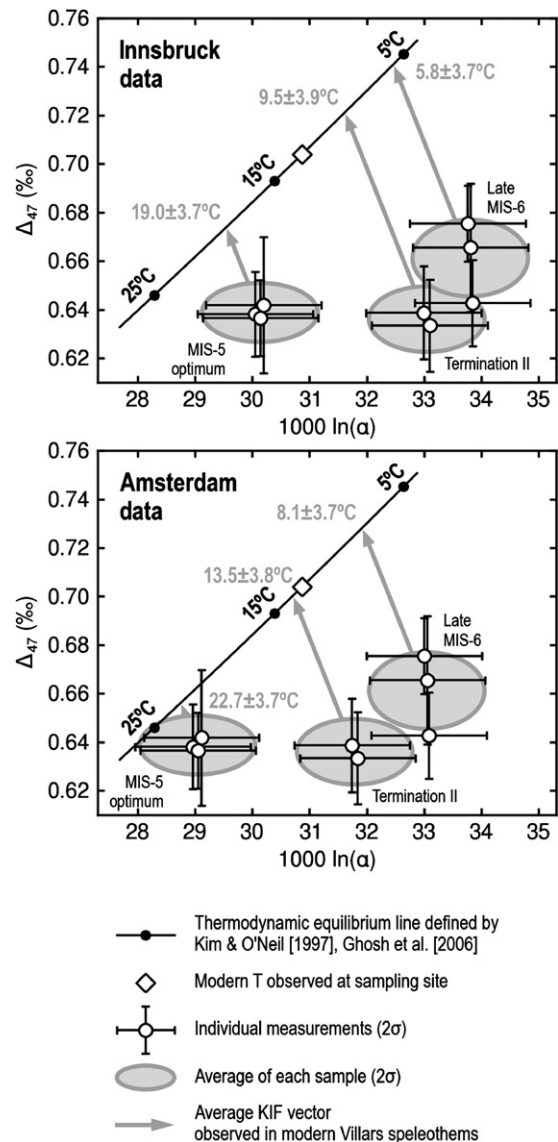


**Fig. 11.** In the 2D space defined by  $1000\ln(\alpha)$  and  $\Delta_{47}$  values, carbonate formed at thermodynamic equilibrium would plot along a specific line defined by existing temperature equations (Kim and O'Neil [1997], Ghosh et al. [2006]). Because of rapid rates of  $\text{CO}_2$  degassing and carbonate precipitation, KIF effects cause the three Vil-car-1 samples to plot below the equilibrium line. Using modern analyses to constrain the slope of past kinetic fractionation vectors, each sample may be projected back onto the equilibrium line to its original crystallization temperature. Note, the overall consistency of relative temperature variations between the 2 datasets, which allows to constrain the warming between Late MIS6 and the last interglacial optimum to  $+13.9 \pm 5.2$  °C ( $2\sigma$ ). Grey ellipses and numerical uncertainties all correspond to  $2\sigma$  confidence limits.

For the time being, although this issue remains somewhat of a limiting factor concerning absolute paleotemperatures, inter-laboratory differences appear by contrast to have little effect on the temperature increase between the end of MIS6 and the Last Interglacial optimum. Using FI data from Innsbruck or Amsterdam respectively yield  $\Delta T[6-5]$  estimates of  $13.2 \pm 2.6$  and  $14.6 \pm 2.6$  °C ( $1\sigma$ ) (Fig. 11).

### c) Comparison with independent constraints

Compared to paleotemperatures derived from  $\delta^{18}\text{O}$  using classical equilibrium fractionation functions (5.1.1 b), our clumped isotope/fluid inclusion reconstructions yield temperatures

consistent with recently published independent estimates. For instance, pollen data from Monticchio Maar indicates a maximum amplitude of  $\sim 12^\circ\text{C}$  between end of MIS6 and the Last Interglacial optimum (Allen and Huntley, 2009). Noble gas fluid inclusion analyses from a western Germany stalagmite yield  $9 \pm 5^\circ\text{C}$  ( $1\sigma$ ) as a lower bound for temperature rise across Termination II (Scholz et al., 2009). Finally, as shown in Fig. 6, this period also saw strong ( $\sim 13^\circ\text{C}$ ) warming in North Atlantic and Western Mediterranean surface waters (Kandiano et al., 2004; Martrat et al., 2004; Sánchez Goñi et al., 2008), and the terrestrial amplitude of glacial/interglacial temperature changes is generally accepted to be larger than that of SST.

The amplitude of the temperature fluctuation in a continental setting in the region at Termination I between the extremes is assumed to be about  $7\text{--}13^\circ\text{C}$  (Allen et al., 1999; McGarry et al., 2004; Wu et al., 2007; Affek et al., 2008) which is consistent with the amplitude of this study as well.

### 5.2. Drip water isotopic composition relative constancy: a tentative explanation

One of our most striking results is the drip water  $\delta^{18}\text{O}$  constancy within  $1\text{‰}$  ( $2\sigma$ ) from early MIS6 to the Last Interglacial  $\delta^{18}\text{O}$  optimum. This was unexpected as the associated  $\delta^{18}\text{O}_c$  decrease by  $5\text{‰}$  and these phenomena occur synchronously to a first order climatic transition. The VU  $\delta^{18}\text{O}_w$  average ( $-6.4\text{‰}$ , Table 2) is consistent with the values measured for modern drip water in the Villars cave (Table 2) and with the  $\delta^{18}\text{O}_w$  of water trapped in macro inclusions of the MIS 5c ( $\sim 101$  ka) portion of the Vil24 stalagmite from Villars Cave ( $-5.9$  to  $-6.1 \pm 0.2\text{‰}$  ( $1\sigma$ ), (Genty et al., 2002)). Thus, it is likely that drip water oxygen isotopic composition did not show significant changes during the last 150 ka. We investigated this observation for the Termination II interval.

As it is currently found in the literature, drip water isotopic composition depends on several factors: (i) isotopic composition of the vapor source, (ii) storm tracks, (iii) air temperature, (iv) rainfall amount effect. There is no particular reason for a change of vapor source or storm track between late MIS6 and the Last Interglacial. Besides, we have demonstrated that rainfall amount effect does not play a dominant role in the rain oxygen isotopic depletion.

From the literature, we know that: (1) During the last deglaciation the ocean isotopic composition decreased by  $1\text{‰}$  (Adkins and Schrag, 2001). We will assume the same amplitude of change for TII; (2) The rain oxygen isotopic composition,  $\delta^{18}\text{O}_R$  versus air temperature gradient is predicted at  $0.58\text{‰}/^\circ\text{C}$  for mid-latitudes (Rozanski et al., 1993). In France, the Thonon-les-bains ( $46^\circ 22' \text{N}$ ,  $6^\circ 28' \text{E}$ , 385 masl) data set between 1963 and 1997 gives a gradient of  $0.37\text{‰}/^\circ\text{C}$  and  $0.20\text{‰}/^\circ\text{C}$  for the Brest ( $48^\circ 36' \text{N}$ ;  $4^\circ 57' \text{W}$ , 80 masl) data set between 1996 and 2000 (IAEA GNIP data). Based on the interpretation of modern rainfall composition and air temperature data accumulated between 1996 and 2006 at Le Mas meteorological station ( $\sim 60$  km SE from Villars), we deduced a seasonal relationship between rainfall oxygen isotopic composition ( $\delta^{18}\text{O}_R$ ) and surface air temperature:  $\delta^{18}\text{O}_R$  ( $\text{‰ SMOW}$ ) =  $0.24 T(^\circ\text{C}) - 9.24$  ( $R^2 = 0.89$ ) (Genty, 2008 and this study). The gradient ( $\sim 0.24\text{‰}/^\circ\text{C}$ ) is consistent with what can be found in previously quoted references and consists of an absolute value close to fractionation factor of the equilibrium formula but with an opposite sign.

We have calculated rainfall oxygen isotopic composition ( $\delta^{18}\text{O}_R$ ) for the two considered periods and we have checked if the different impacts of each factor could cancel out each other during the deglaciation: (1) We have used the local seasonal relationship above and the monthly temperature estimates provided by the coupled model IPSL-CM4 (Marti et al., 2005, submitted for publication), a 3D model atmosphere-ocean-continent and sea ice

at 126 ka for the Villars cave geographic coordinates, to deduce monthly  $\delta^{18}\text{O}_R$  during the Last Interglacial (collaboration with P. Braconnot and E. Mosquet); (2) Assuming the difference of mean annual temperature between the end of MIS6 and the Last Interglacial  $\delta^{18}\text{O}_c$  optimum resulting from this study ( $\Delta T[6-5] = 14^\circ\text{C}$ ), we calculated the late MIS6 monthly temperature (i.e., for January  $T_{\text{Jan}_{126\text{ka}}} - \Delta T[6-5] = T_{\text{Jan}_{\text{MIS6}}}$ ) and monthly rainfall  $\delta^{18}\text{O}_R$  using the local seasonal relationship again; (3) From our model, a temperature rise of  $\sim 14^\circ\text{C}$  between the end of MIS 6 and MIS5 optimum suggests eight months of seasonal freezing that prevent water from infiltrating into the karst during late MIS6. This is consistent with soil structure observed on the studied area (Van Vliet-Lanoë, 1988 and personal communication). By analogy with recent observations for a northern Swedish cave (Sundqvist et al., 2007), we assumed negligible infiltration when the temperature of the month was negative and a rainfall partition similar to what is predicted by the IPSL model at 126 ka which is quite similar as today.

Suppressing the eight months freezing involves a depletion of the drip water  $\delta^{18}\text{O}_w$  of  $\sim -2.7\text{‰}$ . The vapor source  $\delta^{18}\text{O}_{\text{seawater}}$  change between a glacial and interglacial period leads to a depletion of  $\sim -1\text{‰}$  and the air temperature increase would correspond to an enrichment of  $\sim 3.4\text{‰}$  with a gradient of  $0.24\text{‰}/^\circ\text{C}$ . Consequently, the different effects broadly cancel out each other (Supplementary material Figure C). Details for this calculations are discussed in (Wainer, 2009). In order to be more precise, it would be interesting to investigate the rainfall partition along the year as it was attempted by (Meyer et al., 2008), but data to constrain this parameter are lacking.

As the results of the different effects of the factors influencing the  $\delta^{18}\text{O}_w$  that counteract each other, drip water  $\delta^{18}\text{O}_w$  remains more or less constant during the TII. This suggests that the Vil-car-1  $\delta^{18}\text{O}_c$  TII shift depends mostly on temperature rise. This appears to be restricted to Termination II. Indeed, no significant shift is observed in Vil-car-1  $\delta^{18}\text{O}_c$  record for Termination I. A warming amplitude threshold may be involved but fluid inclusion data should be done in the TI part of the core and also on other TII speleothems of the same region in order to confirm this assumption.

### 5.3. Isotopic and geochemical patterns at the MIS6-MIS5 transition

According to the age model the penultimate glacial maximum in Vil-car-1 core corresponds to the d63.5 cm/top discontinuity, after which deposition of calcite resumes (Figs. 2 and 6).

From the discontinuity d63.5 cm/top up to  $\sim 44.7$  cm/top, the calcite appears dark, dense and compact (Fig. 2). The first age obtained after this discontinuity is  $148.3 \pm 4.9$  ka. High values of both  $\delta^{13}\text{C}_c$  and  $\delta^{18}\text{O}_c$  are observed between  $\sim 148.3$  to  $\sim 145.8$  ka (63.5–62.9 cm/top), coinciding with relatively high Mg and Sr concentrations (Fig. 4). One possible explanation is that calcite deposition occurred under cold conditions and/or was associated with prior calcite precipitation in the epikarst which can cause such high values (Fairchild et al., 2000). It will be necessary to check this latter possibility by supplementary trace element measurements in order to establish if a statistical correlation exists. The first warming from 62.9 cm/top ( $145.4 \pm 2.8$  ka), particularly visible for the  $\delta^{13}\text{C}$  signal (depletion of  $3.2\text{‰}$ ) and somewhat subdued on the  $\delta^{18}\text{O}_c$  profile (depletion of  $2\text{‰}$ ), is associated with decreasing Mg and Sr contents.

The warming phase is followed by the two-step deglaciation. The reversal is centred at  $\sim 129.8$  ka on the  $\delta^{18}\text{O}_c$  curve and 128.9 ka for  $\delta^{13}\text{C}$  curve (Fig. 6). A similar pattern consisting of a first warming episode followed by a two-step deglaciation is observed in the  $\delta^{18}\text{O}_c$  profile from Soreq cave (Bar-Matthews et al., 1999, 2003), in M23414 and MD04-2845 Atlantic SST records (Kandiano et al.,

2004; Sánchez Goñi et al., 2008) and in the  $\delta^{18}\text{O}$  benthic record off the Iberian margin (Gouzy et al., 2004) (Figs. 1 and 6).

According to the age model, this feature can be tentatively assigned to the Zeifen/Kattegat (Zeifen/post-Zeifen) oscillation observed in other contemporaneous terrestrial archives (Gruger, 1979; Seidenkrantz et al., 1996; Brauer et al., 2007; Sánchez Goñi, 2007). This cooling is recorded by a decrease of pollen abundance in the Lago Grande di Monticchio between 128.2 and 127.9 ka. Assuming that the  $\delta^{18}\text{O}_c$  variations in the Vil-car-1 core are primarily controlled by the temperature, this  $\delta^{18}\text{O}_c$  reversal back to pre-deglaciation values is consistent with the observation in the northern Atlantic of ice-rafted debris (IRD) deposits and an increase in both benthic and planktonic  $\delta^{18}\text{O}$  during Heinrich event H11 (Lototskaya and Ganssen, 1999; Gouzy et al., 2004). The iceberg discharge linked to this event, synchronous with the post-Zeifen episode, likely caused a significant cooling in Europe and specifically at Villars site which is close to the Atlantic Ocean. This reversal is recorded in a neighbour karstic site as well, Bourgeois-Delaunay Cave (Couchoud et al., 2009).

The observation that this reversal is less pronounced in the  $\delta^{13}\text{C}_c$  than in the  $\delta^{18}\text{O}_c$  record can be explained by the short duration of this event. Despite the significant uncertainties of our dating results in this part of the core, it appears likely that the duration of this episode did not exceed  $\sim 200$  years; this is consistent with its estimated duration in the Monticchio record (250 years; Brauer et al., 2007). The duration of this cooling event was sufficient for the thermic wave to reach the cave but was not long enough to completely annihilate the vegetation but likely reduced its activity. It is interesting to note that no petrographic change is associated to the  $\delta^{18}\text{O}_c$  and  $\delta^{13}\text{C}_c$  drops (Fig. 2).

Regular wiggles of  $\sim 0.8\%$  in amplitude are visible on the  $\delta^{18}\text{O}_c$  descending plateau. It is much less evident in the  $\delta^{13}\text{C}_c$  profile (Figs. 2 and 4). To our knowledge, this cyclicity has not been detected anywhere else, probably because of a lack of records with sufficiently high resolution for this period. According to our age model, these regular cycles have a centennial frequency. Their cause is not yet explained.

## 6. Conclusions

The Vil-car-1 record is the first speleothem record from Villars cave that extends back sufficiently ( $\sim 180$  ka) to record the penultimate deglaciation: the transition between Late MIS 6 and the Last Interglacial “optimum” is prominently recorded as a  $\sim 5\%$  depletion event affecting calcite  $\delta^{18}\text{O}$  values.

Investigation of the potential causes for this isotopic depletion yielded several important results. The oxygen isotope composition of paleodripwater trapped in fluid inclusions before, during and after the transition remains constant (within  $1\%$ ) across the penultimate deglaciation. This observation was independently confirmed by analyses from two different laboratories. This implies that isotopic effects related to the various processes that are expected to affect seepage water compositions during Termination II (changing amount of rainfall, seasonal bias in drip water composition due to winter freezing, etc.) cancelled each other. The  $5\%$  drop in  $\delta^{18}\text{O}_c$  must thus mainly be attributed to an increase in cave temperature during the deglaciation (and to a lesser extent to variation in KIF between late MIS6 and the Last Interglacial optimum). However, using “simple” isotopic paleothermometers ( $\delta^{18}\text{O}$ ,  $\Delta_{47}$ ) to estimate the absolute temperatures before and after this transition yielded unrealistic results, strongly suggesting that calcite deposition occurred in non-equilibrium conditions.

Correcting quantitatively for these isotopic disequilibria was achieved by combining fluid inclusion  $\delta^{18}\text{O}$  analyses with clumped isotope measurements: as described by Guo et al. (submitted for

publication), modern observations can be used to constrain the relationship between kinetic fractionations affecting  $\delta^{18}\text{O}$  and  $\Delta_{47}$ , and thus to reconstruct absolute paleotemperatures. These temperatures range from  $5.5$  or  $7.9$  °C ( $\pm 1.9$  °C,  $1\sigma$ ) during Late MIS6, to  $18.9$  or  $22.9$  °C ( $\pm 1.9$  °C,  $1\sigma$ ) for the Last Interglacial  $\delta^{18}\text{O}_c$  optimum (using fluid inclusion data from UI and VU, respectively). Based on these results, the temperature increase between late MIS6 and the Last Interglacial  $\delta^{18}\text{O}_c$  optimum can be robustly constrained to  $\sim 14$  °C (with a formal standard error of  $2.7$  °C), which appears to be consistent with existing independent estimates from pollen and sea-surface temperature records from Western Europe.

Combined fluid inclusion and clumped isotope analyses thus offer a promising method to reconstruct absolute paleotemperatures from speleothems deposited out of isotopic equilibrium with their parent waters. This new approach now needs to be validated by further studies from well-characterized cave sites.

## Acknowledgements

This work was funded by the CNRS through the ANR PICC program and CNRS INSU programs (ECLIPSE). A significant part of the U–Th dating was done at the GEOTOP laboratory and SEM observations were realised in collaboration with Eric Robin using JEOL JSM 840. We thank the Villars Cave owner, the Versaveau family, O. Mestre for original meteorological data, P. Braconnot and E. Mosquet for the model IPSL-CM4 outputs, F. Mansouri, H. Rebaubier, F. Dewilde for their help with the stable isotopes and trace elements measurements. We are grateful to H. Affek and W. Guo for many hours of fruitful discussion about  $\Delta_{47}$  and equilibrium, as well as D. Hoffman, F. Chabaux, N. Frank, B. Kiefel and V. Plagnes for fruitful discussions about U-series and V. Masson-Delmotte, M.F. Sanchez-Goni and E. Michel for the various exchanges we had about Last Interglacial period and all the scientists whose work appear in this paper for the availability of their data. We are grateful to H. Affek and anonymous reviewer who helped to improve significantly the manuscript. This is LSCE contribution n°4335.

## Appendix

Supplementary data related to this article can be found online at doi:10.1016/j.quascirev.2010.07.004

## References

- Adkins, J.F., Schrag, D.P., 2001. Pore fluid constraints on deep ocean temperature and salinity during the last glacial maximum. *Geophys. Res. Lett.* 28, 771–774.
- Affek, H.P., Guo, W., Daeron, M., Eiler, J.M., 2008. ‘Clumped isotopes’ in speleothem carbonate and atmospheric  $\text{CO}_2$ —is there a kinetic isotope effect? *Geochim. Cosmochim. Acta* 72 A6–A6.
- Allen, J.R.M., Brandt, U., Brauer, A., Hubberten, H.-W., Huntley, B., Keller, J., Kraml, M., Mackensen, A., Mingram, J., Negendank, J.F.W., Nowaczyk, N.R., Oberhänsli, H., Watts, W.A., Wulf, S., Zolitschka, B., 1999. Rapid environmental changes in southern Europe during the last glacial period. *Nature* 400, 740–743.
- Allen, J.R.M., Huntley, B., 2009. Last Interglacial palaeovegetation, palaeoenvironments and chronology: a new record from Lago Grande di Monticchio, southern Italy. *Quaternary Sci. Rev.* 28, 1521–1538.
- Almogi-Labin, A., Bar-Matthews, M., Shriki, D., Kolosovsky, E., Paterne, M., Schilman, B., Ayalon, A., Aizenshtat, Z., Matthews, A., 2009. Climatic variability during the last w90 ka of the southern and northern Levantine Basin as evident from marine records and speleothems. *Quaternary Sci. Rev.* 28, 2882–2896.
- Bar-Matthews, M., Ayalon, A., Kaufman, A., Wasserburg, G.J., 1999. The Eastern Mediterranean paleoclimate as a reflection of regional events: Soreq cave, Israel. *Earth Planet Sc Lett.* 166, 85–95.
- Bar-Matthews, M., Ayalon, A., Gilmour, M., Matthews, A., Hawkesworth Chris, H., 2003. Sea-Land oxygen isotopic relationships from planktonic foraminifera and speleothems in the Eastern Mediterranean region and their implication for paleorainfall during interglacial intervals. *Geochimica Cosmochimica Acta* 67, 3181–3199.
- Beaulieu, J.L.d., Guiot, J., Reille, M., 1991. Long European pollen records and quantitative reconstruction of the last climatic cycle. 1989. In: Goodess, C.M.,

- Palutikof, J.P. (Eds.), Future Climatic Change and Radioactive Waste Disposal. NIREX, Norwich, NSS/R257, pp. 116–136.
- Begemann, F., Ludwig, K.R., Lugmair, G.W., Min, K., Nyquist, L.E., Patchett, P.J., Renne, P.R., Shih, C.Y., Villa, I.M., Walker, R.J., 2001. Call for an improved set of decay constants for geochronological use. *Geochim Cosmochim Acta* 65, 111–121.
- Borsato, A., Frisia, S., Fairchild, I.J., Somogyi, A., Susini, J., 2007. Trace element distribution in annual stalagmite laminae mapped by micrometer-resolution X-ray fluorescence: implications for incorporation of environmentally significant species. *Geochim Cosmochim Acta* 71, 1494–1512.
- Brauer, A., Allen, J.R.M., Mingram, J., Dulski, P., Wulf, S., Huntley, B., 2007. Evidence for last interglacial chronology and environmental change from Southern Europe. *P Natl. Acad. Sci. USA* 104, 450–455.
- van Calsteren, P., Schwieters, J.B., 1995. Performance of a thermal ionization mass spectrometer with a deceleration lens system and post-deceleration detector selection. *Int. J. Mass Spectrom. Ion Process.* 146, 119–129.
- Cheddadi, R., Mamakowa, K., Guiot, J., de Beaulieu, J.L., Reille, M., Andrieu, V., Granoszewski, W., Peyron, O., 1998. Was the climate of the Eemian stable? A quantitative climate reconstruction from seven European pollen records. *Palaeogeography, Palaeoclimatology, Palaeoecology* 143, 73–85.
- Cheddadi, R., de Beaulieu, J.L., Jouzel, J., Andrieu-Ponel, V., Laurent, J.M., Reille, M., Raynaud, D., Bar-Hen, A., 2005. Similarity of vegetation dynamics during interglacial periods. *P Natl. Acad. Sci. USA* 102, 13939–13943.
- Cheng, H., Edwards, R.L., Hoff, J., Gallup, C.D., Richards, D.A., Asmerom, Y., 2000. The half-lives of uranium-234 and thorium-230. *Chem. Geol.* 169, 17–33.
- Cheng, H., Edwards, R.L., Wan, Y.J., Ko, X.G., Ming, Y.F., Kelly, M.J., Wang, X.F., Gallup, C.D., Liu, W.G., 2006. A penultimate glacial monsoon record from Hulu Cave and two-phase glacial terminations. *Geology* 34, 217–220.
- Cleroux, C., Cortijo, E., Anand, P., Labeyrie, L., Bassinot, F., Caillon, N., Duplessy, J.C., 2008. Mg/Ca and Sr/Ca ratios in planktonic foraminifera: Proxies for upper water column temperature reconstruction. *Paleoceanography* 23.
- Combouret-Nebout, N., Turon, J.L., Zahn, R., Capotondi, L., Londeix, L., Pahnke, K., 2002. Enhanced aridity and atmospheric high-pressure stability over the western Mediterranean during the North Atlantic cold events of the past 50 kyr. *Geology* 30, 863–866.
- Coplen, T.B., 2007. Calibration of the calcite-water oxygen-isotope geothermometer at Devils Hole, Nevada, a natural laboratory. *Geochim Cosmochim Acta* 71, 3948–3957.
- Couchoud, I., Genty, D., Hoffmann, D., Drysdale, R., Blamart, D., 2009. Millennial-scale climate variability during the Last Interglacial recorded in a speleothem from south-western France. *Quaternary Sci. Rev.* 28, 3263–3274.
- Craig, H., 1965. The measurement of oxygen isotope paleotemperatures. In: Tongiorgi, E. (Ed.), *Stable Isotopes in Oceanographic Studies and Paleotemperatures*. Consiglio Nazionale delle Ricerche Laboratorio di Geologia Nucleare, Pisa, pp. 166–182.
- Daëron, M., Guo, W., Eiler, J., Genty, K., Blamart, D., Boch, R., Drysdale, R.N., Maire, R., Wainer, K., Zanchetta, G., <sup>13</sup>C/<sup>18</sup>O clumping in speleothems: Observations from natural caves and precipitation experiments, submitted for publication.
- Dorale, J.A., Edwards, R.L., Onac, B.P., 2002. Stable isotopes as environmental indicators in speleothems. In: Daoxian, Y., Cheng, Z. (Eds.), *Karst Processes and the Carbon Cycle*. Final Report of IGCP379. Geological Publishing House, Beijing, China, pp. 107–120.
- Drysdale, R.N., Zanchetta, G., Hellstrom, J.C., Fallick, A.E., Zhao, J.X., 2005. Stalagmite evidence for the onset of the Last Interglacial in southern Europe at  $129 \pm 1$  ka. *Geophys. Res. Lett.* 32.
- Drysdale, R.N., Zanchetta, G., Hellstrom, J.C., Fallick, A.E., McDonald, J., Cartwright, I., 2007. Stalagmite evidence for the precise timing of North Atlantic cold events during the early last glacial. *Geology* 35, 77–80.
- Drysdale, R.N., Hellstrom, J., Zanchetta, G., Fallick, A.E., Sánchez Goñi, M.F., Couchoud, I., McDonald, J., Maas, R., Lohmann, G., Isola, I., 2009. Evidence for obliquity forcing of glacial Termination II. *Science* 325, 1527–1531.
- Dublyansky, Y.V., Spötl, C., 2009. Hydrogen and oxygen isotopes of water from inclusions in minerals: design of a new crushing system and on-line continuous-flow isotope ratio mass spectrometric analysis. *Rapid Commun. Mass Spectrom.* 23, 2605–2613.
- Edwards, R.L., Chen, J.H., Wasserburg, G.J., 1987. <sup>238</sup>U–<sup>234</sup>U–<sup>230</sup>Th–<sup>232</sup>Th systematics and the precise measurement of time over the past 500,000 years. *Earth Planet Sci Lett.* 81, 175–192.
- Eiler, J.M., 2007. “Clumped-isotope” geochemistry – The study of naturally-occurring, multiply-substituted isotopologues. *Earth Planetary Sci. Lett.* 262, 309–327.
- Epstein, S., Buchsbaum, R., Lowenstam, H., Urey, H., 1953. Revised carbonate-water isotopic temperature scale. *Bull. Geol. Soc. America* 64, 1315–1326.
- Fairchild, I.J., Borsato, A., Tooth, A.F., Frisia, S., Hawkesworth, C.J., Huang, Y.M., McDermott, F., Spiro, B., 2000. Controls on trace element (Sr–Mg) compositions of carbonate cave waters: implications for speleothem climatic records. *Chem. Geol.* 166, 255–269.
- Fairchild, I.J., Smith, C.L., Baker, A., Fuller, L., Spötl, C., Mathey, D., McDermott, F., Eimp, 2006. Modification and preservation of environmental signals in speleothems. *Earth-Science Rev.* 75, 105–153.
- Friedman, I., O’Neil, J.R., 1977. Compilation of stable isotope fractionation factors of geochemical interest. In: Fleisher, M. (Ed.), *Data of Geochemistry*. U.S. Geological Survey Professional Paper, 440.
- Genty, D., 2008. Paleoclimate Research in Villars cave (Dordogne, SW-France). *Int. J. Speleology* 37, 173–191.
- Genty, D., Baker, A., Barnes, W., 1997. Comparaison entre les lamines luminescentes et les lamines visibles annuelles de stalagmites. *Comptes Rendus de l’Académie des Sciences de Paris. Sci. de la terre des planètes* 325, 193–200.
- Genty, D., Baker, A., Massault, M., Proctor, C., Gilmour, M., Pons-Branchu, E., Hamelin, B., 2001. Dead carbon in stalagmites: carbonate bedrock paleodissolution vs. ageing of soil organic matter. Implication for <sup>13</sup>C variation in speleothems. *Geochim Cosmochim Acta* 65, 3443–3457.
- Genty, D., Plagnes, V., Causse, C., Cattani, O., Stievenard, M., Falourd, S., Blamart, D., Ouahdi, R., Van-Exter, S., 2002. Fossil water in large stalagmite voids as a tool for paleoprecipitation stable isotope composition reconstruction and paleotemperature calculation. *Chem. Geol.* 184, 83–95.
- Genty, D., Blamart, D., Ouahdi, R., Gilmour, M., Baker, A., Jouzel, J., Van-Exter, S., 2003. Precise dating of Dansgaard-Oeschger climate oscillations in western Europe from stalagmite data. *Nature* 421, 833–837.
- Genty, D., Combouret-Nebout, N., Hatte, C., Blamart, D., Ghaleb, B., Isabella, L., 2005. Rapid climatic changes of the last 90 kyr recorded on the European continent. *Cr Geosci.* 337, 970–982.
- Genty, D., Blamart, D., Ghaleb, B., Plagnes, V., Causse, C., Bakalowicz, M., Zouari, K., Chkir, N., Hellstrom, J., Wainer, K., Bourges, F., 2006. Timing and dynamics of the last deglaciation from European and North African delta C-13 stalagmite profiles – comparison with Chinese and South Hemisphere stalagmites. *Quaternary Sci. Rev.* 25, 2118–2142.
- Genty, D., Massault, M., 1997. Bomb <sup>14</sup>C recorded in laminated speleothems: calculation of dead carbon proportion. *Radiocarbon* 39, 33–48.
- Genty, D., Massault, M., 1999. Carbon transfer dynamics from bomb-<sup>14</sup>C and  $\delta^{13}$ C time series of a laminated stalagmite from SW France – Modelling and comparison with other stalagmite records. *Geochim Cosmochim Acta* 63, 1537–1548.
- Genty, D., Combouret-Nebout, N., Peyron, O., Blamart, D., Wainer, K., Mansuri, F., Ghaleb, B., Isabella, L., Dormoy, I., von Grafenstein, U., Bonelli, S., Landais, A., Brauer, A., 2010. Isotopic characterization of rapid climatic events during OIS3 and OIS4 in Villars Cave stalagmites (SW-France) and correlation with Atlantic and Mediterranean pollen records. *Quaternary Sci. Rev.* 29, 2799–2820.
- Ghosh, P., Adkins, J., Affek, H., Balta, B., Guo, W.F., Schauble, E.A., Schrag, D., Eiler, J.M., 2006. C-13-O-18 bonds in carbonate minerals: a new kind of paleothermometer. *Geochim Cosmochim Acta* 70, 1439–1456.
- Guzy, A., Malaizé, B., Pujol, C., Charlier, K., 2004. Climatic “pause” during Termination II identified in shallow and intermediate waters off the Iberian margin. *Quaternary Sci. Rev.* 23, 1523–1528.
- Govin, A., Michel, E., Labeyrie, L., Waelbroeck, C., Dewilde, F., Jansen, E., 2009. Evidence for northward expansion of Antarctic Bottom Water mass in the Southern Ocean during the last glacial inception. *Paleoceanography* 24.
- Greaves, M., Caillon, N., Rebaubier, H., Bartoli, G., Bohaty, S., Cacho, I., Clarke, L., Cooper, M., Daunt, C., Delaney, D., deMenocal, P., Dutton, A., Eggins, S., Elderfield, H., Garbe-Schoenberg, D., Goddard, E., Green, D., Groeneveld, J., Hastings, D., Hathorne, E., Kimoto, K., Klinkhammer, G., Labeyrie, L., Lea, D.W., Marchitto, T., Martinez-Boti, M.A., Mortyn, P.G., Ni, Y., Nuernberg, D., Paradis, G., Pena, L., Quinn, T., Rosenthal, Y., Russell, A., Sagawa, T., Sosdian, S., Stott, L., Tachikawa, K., Tappa, E., Thunell, R., Wilson, P.A., 2008. Interlaboratory comparison study of calibration standards for foraminiferal Mg/Ca thermometry. *Geochim. Geophys. Geosystems* 9.
- Gruger, E., 1979. Grande Pile Peat Bog – Continuous pollen record for the last 140,000 Years – Comment. *Quaternary Res.* 12, 152–153.
- Guo, W., Daeron, M., Niles, P., Genty, D., Kim, S.T., Vonhof, H., Affek, H., Wainer, K., Blamart, D., Eiler, J., 2008. C-13-O-18 bonds in dissolved inorganic carbon: implications for carbonate clumped isotope thermometry. *Geochim Cosmochim Acta* 72 A336–A336.
- Guo, W., Daëron, M., Niles, P., Goddard, W.A., Eiler, J.M. Isotopic fractionations associated with degassing of CO<sub>2</sub> from aqueous solutions: implications for carbonate clumped isotope thermometry, submitted for publication.
- Hendy, C.H., 1971. The isotopic geochemistry of speleothems – I. The calculation of the effects of different modes of formation on the isotopic composition of speleothems and their applicability as palaeoclimatic indicators. *Geochim Cosmochim Acta* 35, 801–824.
- Kandiano, E.S., Bauch, H.A., Müller, A., 2004. Sea surface temperature variability in the North Atlantic during the last two glacial-interglacial cycles: comparison of faunal, oxygen isotopic, and Mg/Ca-derived records. *Palaeogeography, Palaeoclimatology, Palaeoecology* 204, 145–164.
- Kim, S.T., O’Neil, J.R., 1997. Equilibrium and nonequilibrium oxygen isotope effects in synthetic carbonates. *Geochim Cosmochim Acta* 61, 3461–3475.
- Kühl, N., Litt, T., 2007. Reconstruction of Eemian temperature based on the pollen record of site Gröbern, Germany. *Quaternary Sci. Rev.* 26, 3311–3317.
- Lototskaya, A., Ganssen, G.M., 1999. The structure of termination II (penultimate deglaciation and Eemian) in north Atlantic. *Quaternary Sci. Rev.* 18, 1641–1654.
- Ludwig, K.R., 2003. User’s Manual for Isoplot 3. In: *Berkeley Geochron. Ctr. Spec. Pub.* vol. 4, 77 pp.
- Lundberg, J., Ford, D.C., 1994. Late Pleistocene sea-level change in the Bahamas from mass-spectrometric U-Series dating of Submerged speleothem. *Quaternary Sci. Rev.* 13, 1–14.
- Marshall, D., Ghaleb, B., Countess, R., Gabities, J., 2009. Preliminary paleoclimate reconstruction based on a 12,500 year old speleothem from Vancouver Island, Canada: stable isotopes and U–Th disequilibrium dating. *Quaternary Sci. Rev.* 28, 2507–2513.

- Marti, O., Braconnot, P., Bellier, J., Benschila, R., Bony, S., Brockmann, P., Cadule, P., Caubel, A., Denvil, S., Dufresne, J.-L., Fairhead, L., Filiberti, M.-A., Foujols, M.-A., Fichet, T., Friedlingstein, P., Goosse, H., Grandpeix, J.-Y., Hourdin, F., Krinner, G., Lévy, C., Madec, G., Musat, I., de Noblet, N., Polcher, J., Talandier, C., 2005. The New IPSL Climate System Model: IPSL-CM4. Report No. 26. Institut Pierre Simon Laplace, Paris.
- Marti, O., Braconnot, P., Dufresne, J.-L., Bellier, J., Benschila, R., Bony, S., Brockmann, P., Cadule, P., Caubel, A., Codron, F., de Noblet, N., Denvil, S., Fairhead, L., Fichet, T., Foujols, M.-A., Friedlingstein, P., Goosse, H., Grandpeix, J.-Y., Guilyardi, E., Hourdin, F., Krinner, G., Lévy, C., Madec, G., Mignot, J., Musat, I., Swingedouw, D., Talandier, C. Key features of the IPSL ocean atmosphere model and its sensitivity to atmospheric resolution. *Clim Dynam*, submitted for publication.
- Martrat, B., Grimalt, J.O., Lopez-Martinez, C., Cacho, I., Sierro, F.J., Flores, J.A., Zahn, R., Canals, M., Curtis, J.H., Hodell, D.A., 2004. Abrupt temperature changes in the Western Mediterranean over the past 250,000 years. *Science* 306, 1762–1765.
- Martrat, B., Grimalt, J.O., Shackleton, N.J., de Abreu, L., Hutterli, M.A., Stocker, T.F., 2007. Four climate cycles of recurring deep and surface water destabilizations on the Iberian margin. *Science* 317, 502–507.
- Matthews, A., Ayalon, A., Bar-Matthews, M., 2000. D/H ratios of fluid inclusions of Soreq cave (Israel) speleothems as a guide to the Eastern Mediterranean Meteoric Line. *Chem. Geol.* 166, 183–191.
- McCrea, J., 1950. On the isotopic chemistry of carbonates and a paleotemperature scale. *J. Chem. Phys.* 18, 849–857.
- McDermott, F., Elliott, T.R., Vancalsteren, P., Hawkesworth, C.J., 1993. Measurement of Th-230/Th-232 ratios in Young Volcanic-Rocks by single-sector thermal ionization mass-spectrometry. *Chem. Geol.* 103, 283–292.
- McGarry, S., Bar-Matthews, M., Matthews, A., Vaks, A., Schilman, B., Ayalon, A., 2004. Constraints on hydrological and paleotemperature variations in the Eastern Mediterranean region in the last 140 ka given by the  $\delta D$  values of speleothem fluid inclusions. *Quaternary Sci. Rev.* 23, 919–934.
- Meyer, M.C., Spotl, C., Mangini, A., 2008. The demise of the Last Interglacial recorded in isotopically dated speleothems from the Alps. *Quaternary Sci. Rev.* 27, 476–496.
- NorthGRIPmembers, 2004. High resolution climate record of the Northern hemisphere reaching into the Last Interglacial period. *Nature* 43, 147–151.
- O'Neil, J.R., Clayton, R.N., Mayeda, T.K., 1969. Oxygen isotope fractionation in divalent metal carbonates. *J. Chem. Phys.* 51, 5547–5558.
- Plagnes, V., Causse, C., Genty, D., Paterne, M., Blamart, D., 2002. A discontinuous climatic record from 187 to 74 ka from a speleothem of the Clamouse Cave (south of France). *Earth Planet Sc Lett.* 201, 87–103.
- Rousseau, D.D., Hatte, C., Guiot, J., Duzer, D., Schevin, P., Kukla, G., 2006. Reconstruction of the Grande Pile Eemian using inverse modeling of biomes and delta C-13. *Quaternary Sci. Rev.* 25, 2806–2819.
- Rozanski, K., Araguas-Araguas, L., Gonfiantini, R., 1993. Isotopic patterns in modern Global precipitation, in climate change in continental isotopic records. *Geophys. Monogr.* 78, 1–36.
- Sánchez Goñi, M.F., 2007. Introduction to climate and vegetation in Europe during MIS 5. In: Sirocko, F., Clausen, M., Sánchez Goñi, M.F., Litt, T. (Eds.), *The Climate of Past Interglacials*. Elsevier, Amsterdam, pp. 197–205.
- Sánchez Goñi, M.F., Loutre, M.F., Crucifix, M., Peyron, O., Santos, L., Duprat, J., Malaize, B., Turon, J.L., Peyrouquet, J.P., 2005. Increasing vegetation and climate gradient in Western Europe over the Last Glacial Inception (122–110 ka): data-model comparison. *Earth Planet Sc Lett.* 231, 111–130.
- Sánchez Goñi, M.F., Landais, A., Fletcher, W.J., Naughton, F., Desprat, S., Duprat, J., 2008. Contrasting impacts of Dansgaard-Oeschger events over a western European latitudinal transect modulated by orbital parameters. *Quaternary Sci. Rev.* 27, 1136–1151.
- Scholz, D., Kluge, T., Marx, T., Spötl, C., Schröder-Ritzraun, A., Riechelmann, D., Aeschbach-Hertig, W., Mangini, A., Richter, D.K., Niggemann, S., 2009. Temporal gradient between temperature and the oxygen isotope value of precipitation in the reaily Eemian reconstructed from a sepleothem in western Germany. *Geophys. Res.* 11 abstract.
- Schwarcz, H.P., 1986. Geochronology and isotopic geochemistry of speleothems. In: Fritz, P., Fontes, G. (Eds.), *Handbook of Environmental Isotope Geochemistry*. Elsevier, Amsterdam, pp. 271–303.
- Seidenkrantz, M.S., Bornmalm, L., Johnsen, S.J., Knudsen, K.L., Kuijpers, A., Lauritzen, S.E., Leroy, S.A.G., Mergeai, I., Schweger, C., Van Vliet-Lanoë, B., 1996. Two-step deglaciation at the oxygen isotope stage 6/5e transition: the Zeifen-Kattegat climate oscillation. *Quaternary Sci. Rev.* 15, 63–75.
- Shackleton, N.J., Chapman, M., Sanchez Goñi, M.F., Paillet, D., Lancelot, Y., 2002. The classic marine isotope substage 5e. *Quaternary Res.* 58, 14–16.
- Sharp, Z.D., Atudorei, V., Durakiewicz, T., 2001. A rapid method for determination of hydrogen and oxygen isotope ratios from water and hydrous minerals. *Chem. Geol.* 178, 197–210.
- Sundqvist, H.S., Seibert, J., Holmgren, K., 2007. Understanding conditions behind speleothem formation in Korallgrottan, northwestern Sweden. *J. Hydrol.* 347, 13–22.
- Turner, S., van Calsteren, P., Vigier, N., Thomas, L., 2001. Determination of thorium and uranium isotope ratios in low-concentration geological materials using a fixed multi-collector-ICP-MS. *J. Anal. At. Spectrom.* 16, 612–615.
- Vaks, A., Bar-Matthews, M., Ayalon, A., Matthews, A., Frumkin, A., Dayan, U., Halicz, L., Almogi-Labin, A., Schilman, B., 2006. Paleoclimate and location of the border between Mediterranean climate region and the Sahara-Arabian Desert as revealed by speleothems from the northern Negev Desert, Israel. *Earth Planet Sc Lett.* 249, 384–399.
- Van Vliet-Lanoë, B., 1988. Des traces de glace de ségrégation dans la grotte de Remouchamps (Belgique): conséquences en ce qui concerne la sédimentation et la paléoclimatologie. *Ann. de la Société Géologique de Belgique* 111.
- Verheyden, S., 2001. Speleothems as Palaeoclimatic Archives. *Vrije Universiteit, Brussel*, p. 131.
- Vimeux, F., Cuffey, K.M., Jouzel, J., 2002. New insights into Southern Hemisphere temperature changes from Vostok ice cores using deuterium excess correction. *Earth Planet Sc Lett.* 203, 829–843.
- Vogel, J.C., Kronfeld, J., 1997. Calibration of radiocarbon dates for the late Pleistocene using U/Th dates on stalagmites. *Radiocarbon* 39, 27–32.
- Vonhof, H.B., van Breukelen, M.R., Postma, O., Rowe, P.J., Atkinson, T.C., Kroon, D., 2006. A continuous-flow crushing device for on-line delta H-2 analysis of fluid inclusion water in speleothems. *Rapid Commun. Mass Spectrom.* 20, 2553–2558.
- Vonhof, H.B., Atkinson, T.C., van Breukelen, M.R., Postma, O., 2007. Fluid inclusion hydrogen and oxygen isotope analysis using the "Amsterdam Device": a progress report. *Geophys. Res.* 9 Abstract.
- Wainer, K., 2009. Reconstruction climatique des derniers 200ka à partir de l'étude isotopique et géochimique des spéléothèmes du sud de la France. Thèse de doctorat: Université Paris XI.
- Wainer, K., Genty, D., Blamart, D., Hoffmann, D., Couchoud, I., 2009. A new stage 3 millennial climatic variability record from a SW France speleothem. *Palaeogeogr Palaeoclimatol.* 271, 130–139.
- Wang, Y.J., Cheng, H., Edwards, R.L., Kong, X.G., Shao, X.H., Chen, S.T., Wu, J.Y., Jiang, X.Y., Wang, X.F., An, Z.S., 2008. Millennial- and orbital-scale changes in the East Asian monsoon over the past 224,000 years. *Nature* 451, 1090–1093.
- Wu, H.B., Guiot, J.L., Brewer, S., Guo, Z.T., 2007. Climatic changes in Eurasia and Africa at the last glacial maximum and mid-Holocene: reconstruction from pollen data using inverse vegetation modelling. *Clim. Dynam.* 29, 211–229.
- Yuan, D.X., Cheng, H., Edwards, R.L., Dykoski, C.A., Kelly, M.J., Zhang, M.L., Qing, J.M., Lin, Y.S., Wang, Y.J., Wu, J.Y., Dorale, J.A., An, Z.S., Cai, Y.J., 2004. Timing, duration, and transitions of the last interglacial Asian monsoon. *Science* 304, 575–578.